TECHNICAL REPORT STANDARD TITLE PAGE

1. Report No.	2. Government Accession No.	3. Recipient's Catalog No.
TX-95 1966-1F		

4. Title and Subtitle	5. Report Date
Determination of Pavement Thickness with a New Ultrasonic Device	January, 1995
	6. Performing Organization Code

7. Author(s)	8. Performing Organization Report No.
Baker, M.R., Crain, K. and Nazarian S.	Research Report 1966-1F

9. Performing Organization Name and Address	10. Work Unit No.
Center for Geotechnical and Highway Materials Research The University of Texas at El Paso El Paso, Texas 79968-0516	11. Contract or Grant No. Study No. 7-1966

12. Sponsoring Agency Name and Address	13. Type of Report and Period Covered
Texas Department of Transportation P.O. Box 5080 Austin, Texas 78763	Final Report Sept. 1, 1992-Aug 31, 1994
	14. Sponsoring Agency Code

15. Supplementary Notes

Research Performed in Cooperation with TxDOT
Research Study Title: Determination of Thickness of PCC Slabs

16. Abstract

The TxDOT spends a significant amount of money and effort to perform concrete coring. Coring is normally done to monitor the thickness and/or quality of PCC slabs during construction. Because a considerable amount of time is required to perform the procedure, it is done at widely spaced intervals. As a result, the most critical points, in terms of strength or thickness, are sometimes not tested.

The development of reliable and fast nondestructive testing equipment capable of determining the thickness and quality of concrete is desirable. With it, slabs could be tested at closely spaced points and at a fraction of the cost and time of coring.

UTEP, under a contract with SHRP, has developed a comprehensive NDT device to diagnose problems with pavement at early stages. As part of the SHRP project, a technique for determining the thickness of PCC slabs has been implemented. This technology has been packaged as an inexpensive device for nondestructively determining the thickness of PCC slabs.

17. Key Words	18. Distribution Statement
Modulus, Thickness, Nondestructive Testing, Seismic Methods, Quality Control	No restrictions. This document is available to the public through the National Technical Information Service, 5285 Port Royal Road, Springfield, Virginia 22161

19. Security Classif. (of this report)	20. Security Classif. (of this page)	21. No. of Pages	22. Price
Unclassified	Unclassified	53	

Form DOT F 1700.7 (8-69)

Determination of Pavement Thickness with a New Ultrasonic Device

by

Mark R. Baker, Ph.D.

Kevin Crain, M.S.

and

Soheil Nazarian, Ph.D., P.E.

Research Project 7-1966

Determination of Thickness of PCC Slabs

Conducted for

Texas Department of Transportation

The Center for Geotechnical and Highway Materials Research
The University of Texas at El Paso
El Paso, TX 79968-0516
Research Report 1966-1F
August, 1995

Acknowledgements

The authors would like to offer their sincere appreciation to Robert C. Briggs, Jeff Demon Jackson, and Mark McDaniel of the TxDOT Design Division for their support. Thanks are also due to all personnel of the Pavement Evaluation Group, especially Carl Bertrand.

The contents of this report reflect the view of the authors, who are responsible for the facts and accuracy of the data presented herein. The contents do not necessarily reflect the official views or policies of the Texas Department of Transportation. This report does not constitute a standard, specification, or regulation.

NOT INTENDED FOR CONSTRUCTION, BIDDING, OR PERMIT PURPOSES

Mark R. Baker, Ph.D.
Kevin Crain, M.S.
Soheil Nazarian, Ph.D., P.E. (69263)

Abstract

An instrument used primarily to monitor the thickness of PCC slabs has been designed. In addition, the device provides information about the quality of concrete.

The quality and the thickness are determined by estimating Young's and shear modui in the PCC from the following wave propagation measurements:

1) Impact Echo,
2) Ultrasonic Surface Wave, and
3) Ultrasonic Body Wave Velocity.

The instrument designed and constructed to make these measurements contains two accelerometers. Data acquisition, instrument control, and interpretation are computer controlled, with measurements and interpretations reported in both screen and database formats.

In this report, the construction of the device is described. The problems associated with it are also discussed, along with the results from several field testing programs. In general, it was found that the device is quite promising but needs some modifications. These modifications are currently being implemented.

Implementation Statement

At this time, the implementation of this study's results is quite possible. A prototype of the device has been delivered to TxDOT, along with the necessary software packages. In our opinion, the findings should be immediately implemented on a trial basis so that any logistical or practical problems associated with the device or algorithms can be addressed.

Table of Contents

List of Figures

List of Tables

1

Introduction

The Texas Department of Transportation spends a significant amount of money and effort to perform concrete coring. Coring is normally done to monitor the thickness and/or quality of PCC slabs during construction. Because a considerable amount of time is required to perform the procedure, it is done at widely spaced intervals. As a result, the most critical points, in terms of strength or thickness, are sometimes not tested.

The development of reliable and fast nondestructive testing equipment capable of determining the thickness and quality of concrete is desirable. With it, slabs could be tested at closely spaced points and at a fraction of the cost and time of coring.

UTEP, under contract with SHRP, has developed a comprehensive NDT device to diagnose problems with pavement at early stages. As part of the SHRP project, a technique for determining the thickness of PCC slabs has been implemented. This technology has been packaged as an inexpensive device for nondestructively determining the thickness of PCC slabs.

This report contains the status of a new device called the Lunch Box. The report is divided into three major topics: 1) overview, 2) design of the Lunch Box, and 3) field testing of the Lunch Box.

The overview contains a brief description of the parameters to be measured and the theoretical basis for the device.

The conceptual and subsystem design of the device are then described. Basically, the conceptual design deals with how the Lunch Box is used and how the operator is supposed to

interact with it. In the subsystem design, the design of the different components of the Lunch Box is discussed.

The results from field testing with the Lunch Box at several sites are described next. The outcome of these tests was instrumental in understanding some of the advantages and problems with the device.

2

Wave Propagation

For engineering purposes, most pavement sections can be approximated by a layered half-space with reasonable accuracy. With this approximation, the profiles are assumed to be homogeneous and extend to infinity in the horizontal direction and heterogenous in the vertical direction. This heterogeneity is often modelled by a number of layers, each having its own constant properties. In addition, it is assumed that the material in each layer is elastic and isotropic.

In this chapter, the principles of wave propagation are briefly introduced. Relationships between wave velocities and moduli are clarified.

Seismic Body Waves

Wave motion created by a disturbance within an ideal whole-space can be described by two kinds of waves: compression and shear. These waves are collectively called body waves, as they travel within the body of a medium. Compression and shear waves are distinguished by the direction of particle motion relative to the direction of wave propagation.

Compression waves (also called dilatational waves, primary waves, or P-waves) exhibit a push-pull motion. As a result, wave propagation and particle motion are in the same direction, as shown in Figure 2.1a. Compression waves travel faster than other types of waves and, hence, appear first in a direct travel time record.

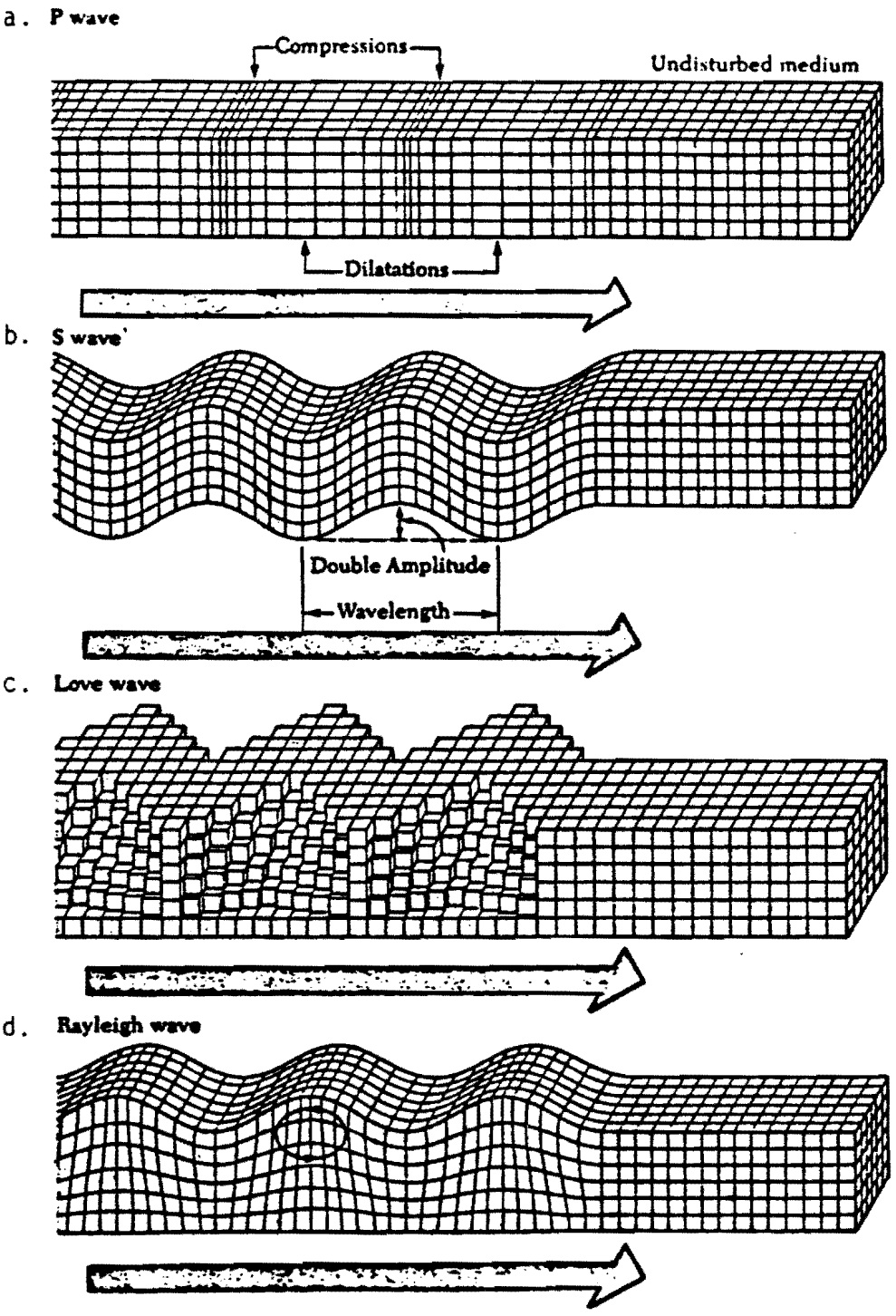

Figure 2.1 - Characteristic Motion of Seismic Waves (from Bolt, 1976)

Shear waves (also called distortional waves, secondary waves, or S-waves) generate a shearing motion, which causes particle motion to occur perpendicular to the direction of wave propagation, as shown in Figure 2.1b. Shear waves can be polarized. If the directions of propagation and particle motion are contained in a vertical plane, the wave is said to be vertically polarized and is called an SV-wave. However, if the direction of particle motion is perpendicular to a vertical plane containing the direction of propagation, the wave is said to be horizontally polarized. This wave is termed an SH-wave. Shear waves travel slower than P-waves and thus appear as the second major wave type in a direct travel time record.

Seismic Surface Waves

In a half-space, waves other than body waves are created. These waves are called surface waves. Many different types of surface waves have been identified and described. The two major types are Rayleigh and Love waves.

Surface waves propagate near the surface of the half-space. Rayleigh waves (R-waves) propagate at a speed of approximately 90 percent of S-waves. Particle motion associated with R-waves is composed of both vertical and horizontal components which, when combined, form a retrograde ellipse close to the surface (see Figure 2.1d). However, with depth, R-wave particle motion changes to purely vertical and, finally, to a prograde ellipse, as illustrated in Figure 2.2. The amplitude of motion attenuates quite rapidly with depth. At a depth equal to about 1.5 times the wavelength, the vertical component of the amplitude is approximately equal to 10% of the original amplitude at the ground surface.

Particle motion associated with Love waves is confined to a horizontal plane and is perpendicular to the direction of wave propagation, as shown in Figure 2.1c. This type of surface wave can only exist when low-velocity layers are underlain by higher-velocity layers, since the waves are generated by total multiple reflections between the top and bottom surfaces of the low-velocity layer. As such, Love waves are not generated in pavement sections.

The propagation of body waves (shear and compression waves) and surface waves (Rayleigh waves) away from a vertically vibrating circular source at the surface of a homogeneous, isotropic, elastic half-space is shown in Figure 2.3. Miller and Pursey (1955) found that, for the situation shown in Figure 2.3, approximately 67 percent of the input energy propagates in the form of R-waves. Shear and compression waves carry 26 and 7 percent of the energy, respectively. Compression and shear waves propagate radically outward from the source. R-waves propagate along a cylindrical wavefront near the surface. Although body waves travel faster than surface waves, body waves attenuate in proportion to $1/r^2$, where r is the distance from the source. Surface wave amplitude decreases in proportion to $1/r^{0.5}$.

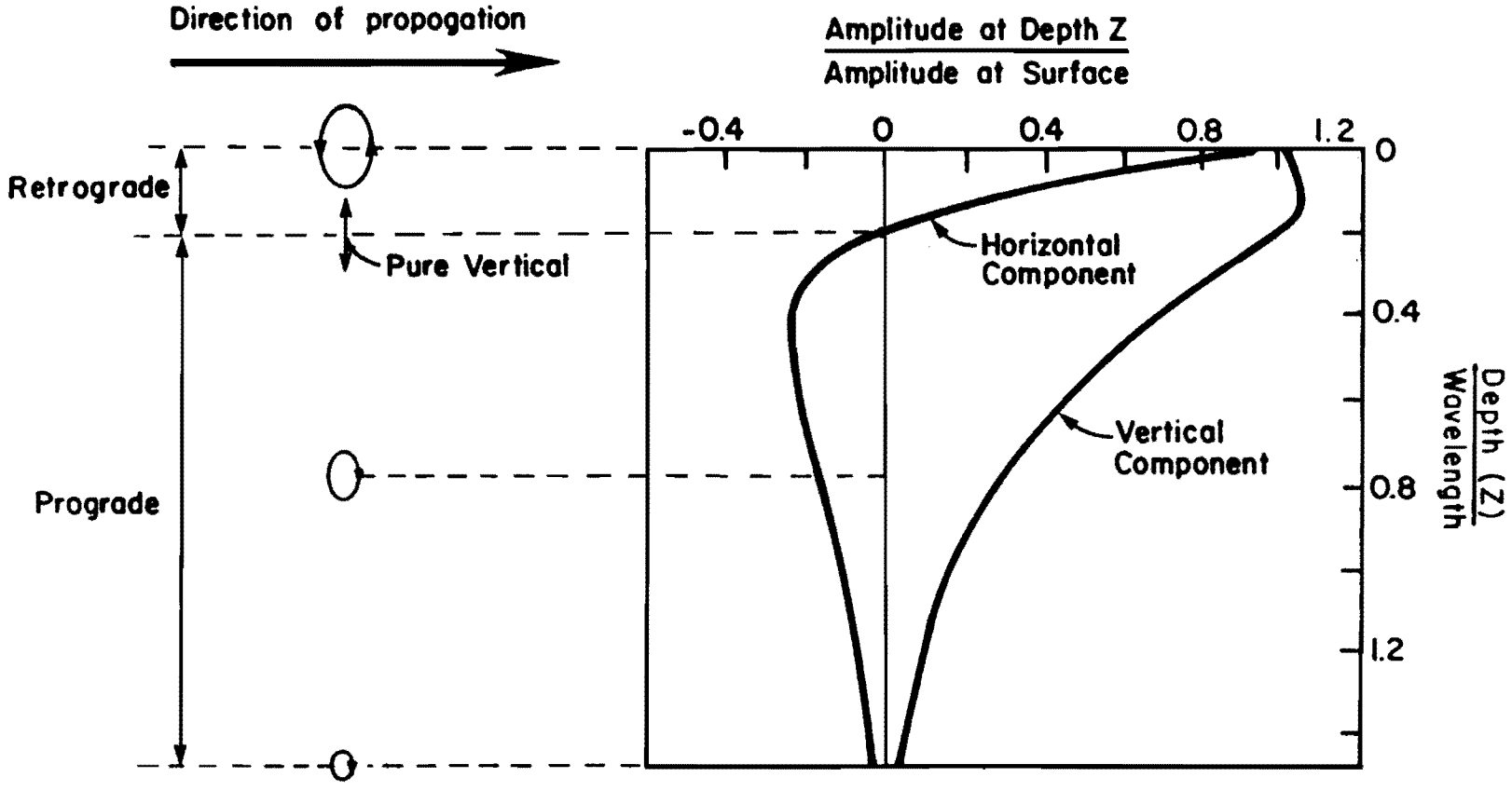

Figure 2.2 - Amplitude and Particle Motion Distribution with Depth for Rayleigh Waves

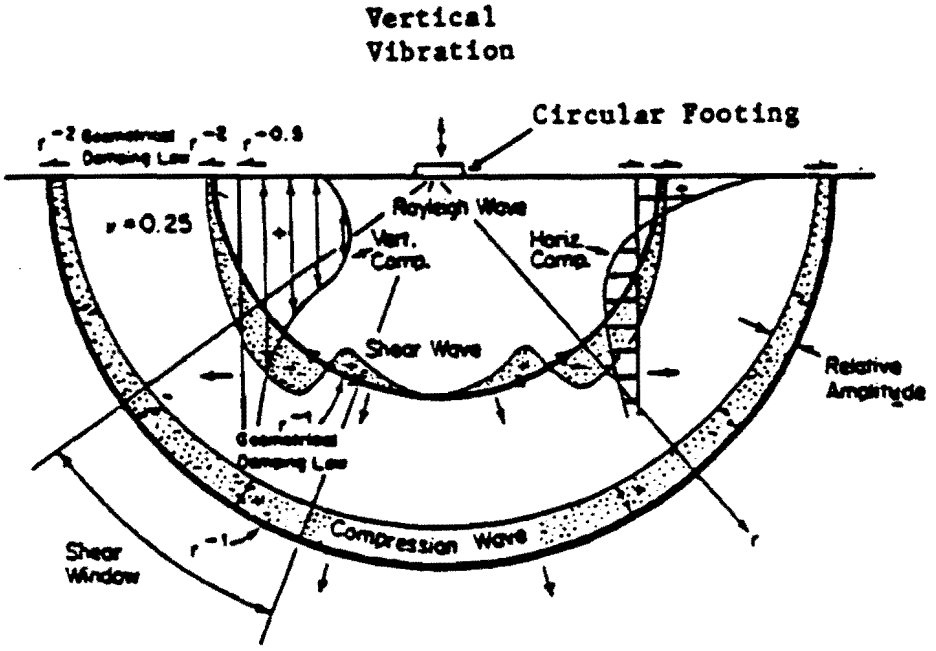

Figure 2.3 - Distribution of Rayleigh, Shear, and Compression Wave Displacements (from Richart et al, 1970)

Seismic Wave Velocities

Seismic wave velocity is defined as the speed at which a wave advances in a medium. Wave velocity is a direct indication of the stiffness of the material; higher wave velocities are associated with higher stiffness. By employing the elastic theory, compression wave velocity can be defined as

$$V_p = \sqrt{\frac{\lambda+2G}{\rho}}, \qquad (2.1)$$

where

V_p = compression wave velocity,
λ = Lame's constant,
G = shear modulus, and
ρ = mass density.

Shear wave velocity, V_s, is equal to

$$V_s = \sqrt{\frac{G}{\rho}}. \qquad (2.2)$$

Compression and shear wave velocities are theoretically interrelated by Poisson's ratio.

The relation can be expressed as

$$\frac{V_s}{V_p} = \sqrt{\frac{0.5-\nu}{1-\nu}}, \qquad (2.3)$$

where υ is the Poisson's ratio. A graphic illustration of Eq. 2.3 is shown in Figure 2.4. For a constant shear wave velocity, compression wave velocity increases with an increase in Poisson's ratio. For a υ of zero, the ratio of V_p to V_s is equal to $\sqrt{2}$; for a υ of 0.5 (an incompressible material), the ratio is equal to infinity.

For a layer with constant properties, R-wave velocity and shear wave velocity are related by Poisson's ratio as well. Although the ratio of R-wave to S-wave velocities increases as Poisson's ratio increases, its change is not significant, as shown in Figure 2.5. For Poisson's ratios of zero and 0.5, this ratio changes from approximately 0.86 to 0.95, respectively. Therefore, it can be assumed that, without introducing an error larger than about five percent, the ratio is equal to 0.90.

Equation 2.3 can be rewritten as

$$\nu = \frac{0.5-(\frac{V_s}{V_p})^2}{1-(\frac{V_s}{V_p})^2}. \qquad (2.4)$$

Elastic Constants

Propagation velocities, per se, have limited use in engineering applications. In pavement engineering, the Young's moduli of different layers should be measured. Calculation of elastic moduli from propagation velocities is, thus, important.

Shear wave velocity, V_s, is used to calculate shear modulus, G, by

$$G = \rho \cdot V_s^2, \qquad (2.5)$$

where ρ is the mass density. Mass density is equal to T_t/g, where T_t is the total unit weight of the material, and g is the gravitational acceleration. If Poisson's ratio (or compression wave velocity) is known, other moduli can be calculated for a given V_s. Young's and shear moduli are related by

$$E = 2G(1+\nu) \qquad (2.6)$$

or

$$E = 2\rho V_s^2(1+\nu). \qquad (2.7)$$

In a medium where the material is restricted from deformation in two lateral directions, the ratio of axial stress to axial strain is called constrained modulus. Constrained modulus, M, is defined as

$$M = \rho V_p^2 \qquad (2.8)$$

or, in terms of Young's modulus and Poisson's ratio,

$$M = \frac{(1-\nu)E}{[1+\nu)(1-2\nu)]}. \qquad (2.9)$$

Bulk modulus, B, is the ratio of hydrostatic stress to volumetric strain and can be determined by

$$B = M - 4/3G. \tag{2.10}$$

3

Principles of Operation

This chapter contains an overview of the measurements made with the Lunch Box. The major topics covered are the parameters measured and the interpretation techniques.

Operational Aspects of Lunch Box

Three different seismic testing techniques are utilized. These tests are

1. Ultrasonic Body Wave (UBW) method,
2. Ultrasonic Surface Wave (USW) method, and
3. Impact Echo (IE) method.

These tests are utilized to determine the thickness and quality of concrete. The parameters calculated from the raw data are summarized in Table 3.1.

Table 3.1 - Strengths of Testing Techniques Utilized in the Lunch Box

Testing Technique	Parameter Measured
Ultrasonic Body Wave	Young's Modulus of top paving layer
Ultrasonic Surface Wave	Shear modulus of top paving layer
Impact Echo	Thickness of paving layer or depth to delaminated layer

A picture of the Lunch Box is shown in Figure 3.1. Two accelerometers (A1 and A2) and a high-frequency source (HFS) are utilized. The receivers and load cell are connected to a data acquisition system.

Upon situating the Lunch Box at a given test location and initiating the testing sequence through use of the computer, the high-frequency source is activated.

The source is fired four to seven times. For the last three impacts of the source, the output voltages of the load cell and receivers are saved and averaged (stacked) in the frequency domain. The other (prerecorded) impacts are used to adjust the gains of the pre-amplifiers. The gains are set in such a manner that the output of the sensors is optimized.

Typical voltage outputs of the two accelerometers are shown in Figure 3.2a. Naturally, as the distance from the source increases, the amplitude of the signal decreases.

To ensure that an adequate signal-to-noise ratio is achieved in all channels, the signals shown in Figure 3.2a are all normalized to a maximum amplitude of one, as shown in Figure 3.2b. In this manner, the main features of the signals can be easily inspected. The signal-to-noise ratios are quite adequate, and the signals follow the classical pattern of waves propagating in the paving layers.

The data collected in this fashion have to be processed utilizing the signal processing and spectral analyses. These processes are described in the next section.

Impact Echo (IE) Method

Upon impact of the slab on the surface, seismic waves which propagate within the PCC slab are generated. Some of the energy is transmitted to the layers underlying the concrete; the remainder is reflected from the boundary of the concrete and underlying layers. The reflected energy will once again reflect at the top of the concrete layer. In this case, almost all the energy will be reflected because of the significant mismatch between the stiffness of air and concrete. Therefore, the reflection of energy will be measured several times by this receiver.

The upper record in Figure 3.2b, which corresponds to the response of the accelerometer placed 75 mm away from the source, is used in the IE tests. The direct arrival of the energy, as well as several reflections, is apparent. The thickness of the slab, H, can be determined from

$$H = (V_p \cdot t_r) / 2, \tag{3.1}$$

where V_p and t_r are the compression wave velocity and travel time between two consecutive reflection arrivals, respectively. The advantage of this method, called Impact Echo (IE), is its simplicity. However, its automation is rather complicated. Another problem with it is

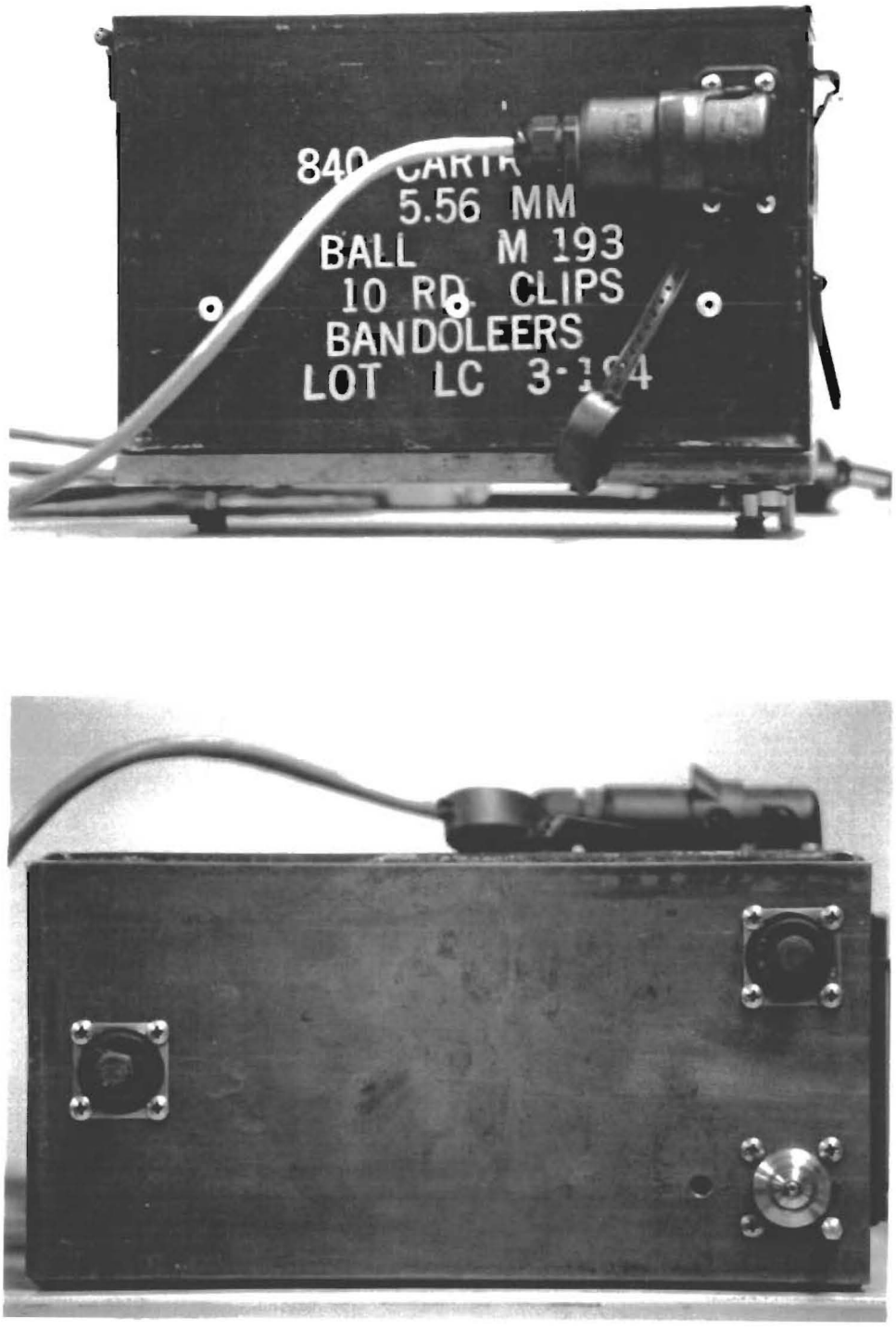

Figure 3.1 - Photograph of Lunch Box

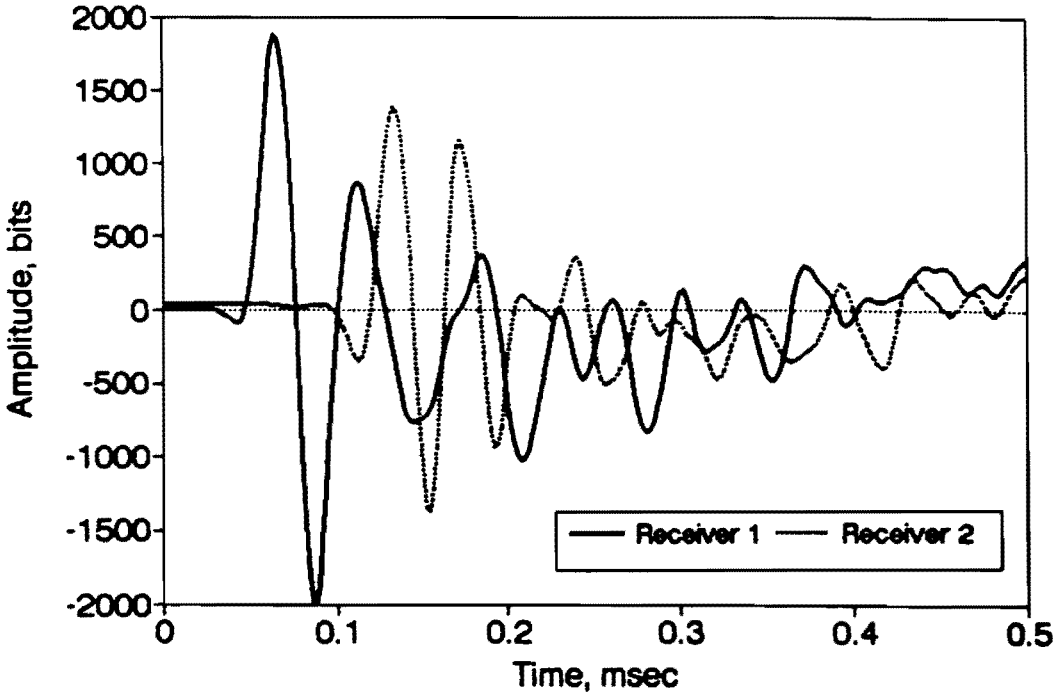

a) Actual Time Records

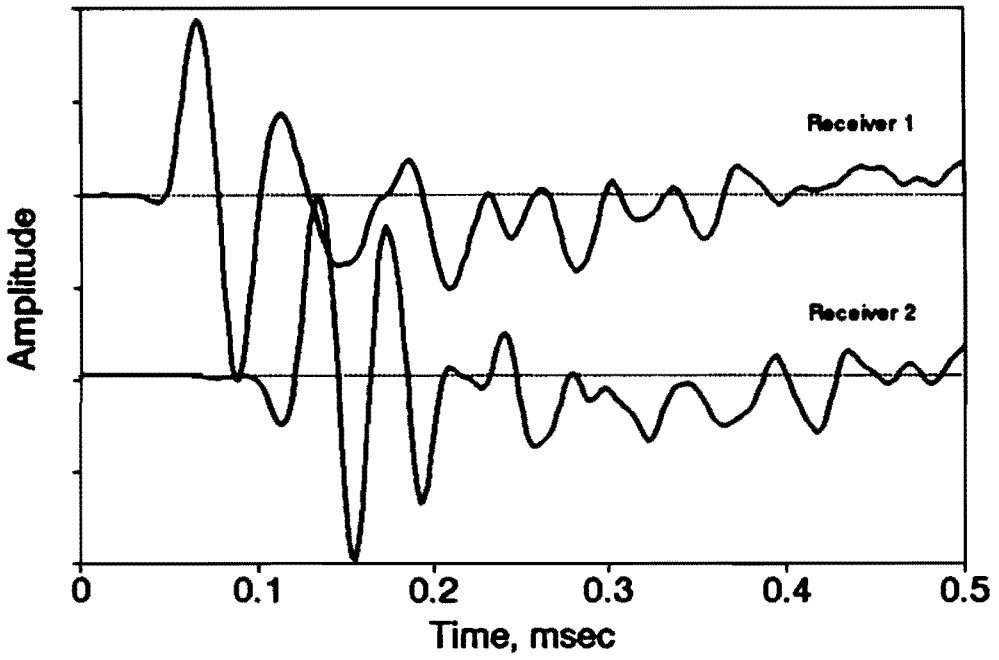

b) Normalized Time Records

Figure 3.2 - Typical Time-Domain Records Collected by Lunch Box

that, in many instances, the separation of the energy related to the direct arrival from the reflected energy is difficult. This frequently happens when the thickness of the slab is thin relative to the wavelength of the energy coupled to the pavement.

The process is made significantly simpler when the signal is transformed in the frequency domain. In this process, the accelerometer signal (such as the one shown in Figure 3.2) is Fourier-transformed. The Fourier-transformed signal for the record shown in Figure 3.2 is shown in Figure 3.3. The plot contains a peak with a significantly high amplitude. This peak, which is called the return (resonant) frequency, is theoretically equal to the reciprocal of t_r. Therefore, the thickness can be determined from

$$H = V_p / 2f_r, \tag{3.2}$$

where f_r is the return (resonant) frequency.

Determining the thickness of a concrete slab using the impact echo method has been thoroughly studied by researchers at the National Institute of Standards and Technology (formerly the National Bureau of Standards). In a comprehensive theoretical and experimental study, Sansalone and Carino (1986) considered the effects of the (1) type of impact source, (2) distance from the impact point to receiver, (3) type of receiving transducer, and (4) depth of reflecting interfaces.

Two major peaks can be seen in Figure 3.3. The one at about 16 kHz corresponds to the thickness of the layer and is called the return (resonant) frequency.

The second peak at about 2 kHz may have resulted for several reasons. It may have been due to pavement-sensor interaction resonance or the flexural (beam) mode of vibration of pavement. This matter is undergoing intense analytical study for better understanding.

The amplitude of the peak is directly related to the mismatch in impedence between the two materials on the two sides of an interface. The impedence of a material is defined as the product of the wave velocity and mass density. Air has an impedence close to zero. The impedence of a regular soil is about 500,000 to 1 million kg/sec-m^2, and concrete typically has an impedence of 10 million kg/sec-m^2.

The larger the mismatch in impedence is, the larger the amplitude of the return resonant frequency will be. On the other hand, if two materials have very similar impedences, virtually no energy will be reflected, and therefore, no resonant return frequency can be measured.

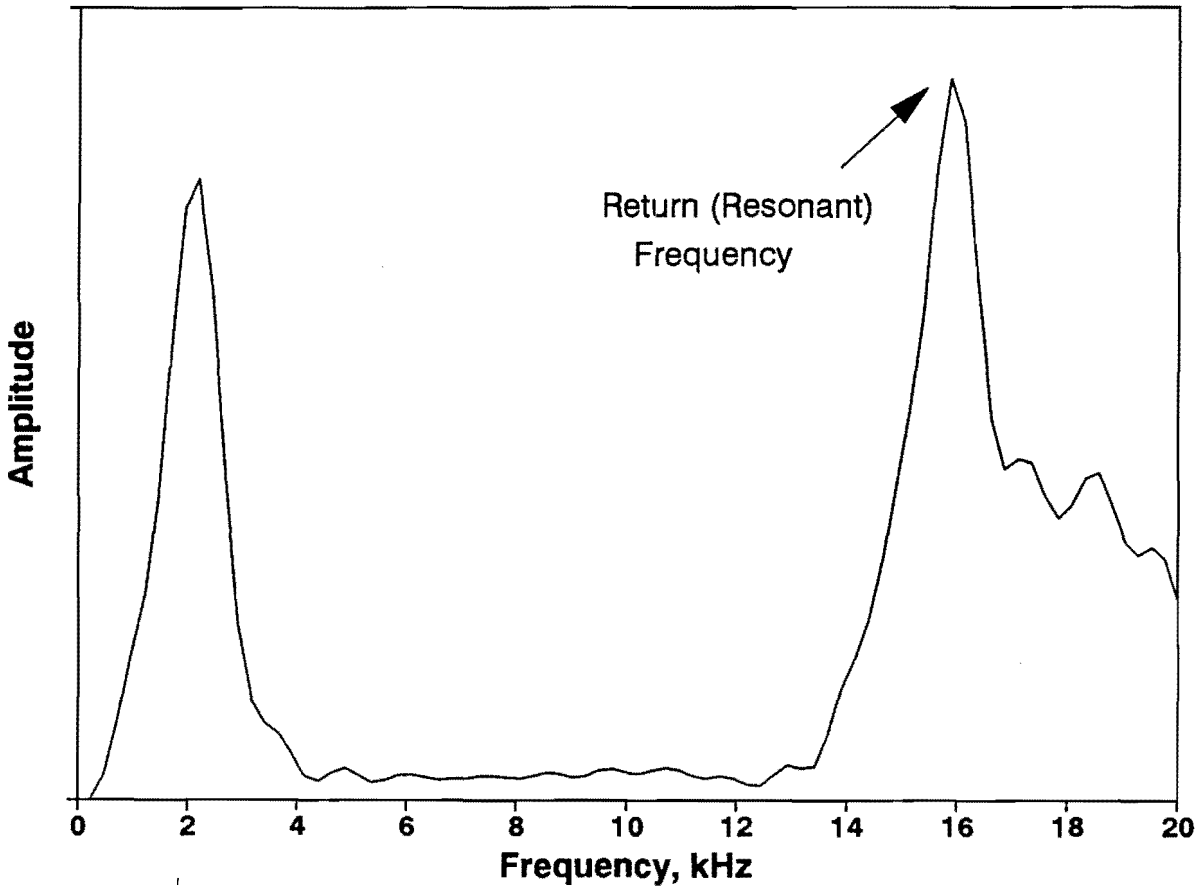

Figure 3.3 - Typical Frequency-Domain Presentation of IE Results

To determine thickness, the following steps should be taken. The compression wave velocity of the material should be determined using the ultrasonic body wave method. Knowing the compression wave velocity and return resonant frequency will allow the thickness to be found. The thickness is simply equal to one-half of the ratio of the compression wave velocity to the return frequency.

Ultrasonic Body Wave (UBW) Method

According to Eq. 3.2, to effectively utilize the IE method, the compression wave velocity of the concrete should be known. This is found using the ultrasonic body wave method. As indicated in Chapter 2, Miller and Pursey (1955) found that when the surface of a medium is disturbed, the generated stress waves propagate mostly with Rayleigh wave energy and, to a lesser extent, shear and compression wave energy. As such, body wave energy present in a seismic record generated using the setup shown in Figure 3.1 is very small. However, compression waves travel faster than any other type of seismic waves and are detected first on seismic records. Several automated techniques for determining the arrival of compression waves are available. A method suggested by Willis and Toksoz (1983) has been implemented in this equipment.

With this method, the detection of P-wave arrival is done in two steps: 1) event detection, and 2) fine adjustment.

Event detection is carried out by triggering on the first amplitude that falls within a time window which satisfies a predetermined amplitude threshold. To implement this step, a detection threshold level is defined. The threshold value depends upon the background noise and anticipated amplitude of the compression wave. This value is typically set as the average of the voltage levels of the background noise and half the anticipated maximum amplitude of the P-wave.

The user defines a window within which the compression wave velocity energy is most likely to be concentrated. This is done by defining the most likely value and possible range for the modulus of the PCC. The first point within the defined window that has a voltage above the threshold is considered a candidate for the arrival of the P-wave. To verify that the arrival of the wave is correctly determined, the second step is carried out.

In the second step, one takes advantage of the fact that the characteristics of the Lunch Box source are well defined. A semblance correlation is carried out between the picks selected for different records. Semblance is used because it discriminates against amplitude differences, as well as the shape of the signal corresponding to the compression wave energy.

This two-step procedure not only yields a relatively robust procedure for determining the compression wave velocity but also determines if the arrival times have been falsely selected because of uncorrelated changes in the background noise level.

Typical time domain records from the two receivers are shown in Figure 3.4a. To clearly detect the arrival of P-waves, the records are greatly amplified, as shown in Figure 3.4b. In the Lunch Box operation, this is achieved by automatically setting the gains of the sensors' amplifiers to maximum. In other words, the data used for determining the P-wave arrival are collected separately.

The arrows in each record in Figure 3.4b correspond to the arrival of compression waves. The compression wave velocity is calculated from the distance between the receivers and the difference in travel time. The compression wave velocity can then be converted to Young's modulus, as discussed in Chapter 2.

Ultrasonic Surface Wave (USW) Method

The ultrasonic surface wave method is an offshoot of the SASW method. The major distinction between these two methods is that, with the USW method, the properties of the top paving layer can be easily and directly determined without the need for a complex inversion algorithm.

To perform the test, a disturbance is applied to the ground surface to generate stress waves which propagate mostly as surface waves of various wavelengths. The waves are monitored and captured with a data acquisition system (through the receivers). Signal and spectral analyses are then utilized to determine the phase information of the cross power spectra (CPS) and the coherence functions among consecutive adjacent receivers. This information is used to develop a dispersion curve. A dispersion curve depicts the variation in the velocity of propagation with wavelength.

To obtain the dispersion curve, the velocity of propagation, V_{ph}, and wavelength, L_{ph}, are determined from the phase of the CPS, ϕ, at any frequency, f. This relationship can be written as

$$V_{ph} = D/[\phi/360f] \tag{3.4}$$

$$L_{ph} = D/[\phi/360], \tag{3.5}$$

where D is the distance between the receivers.

A theoretical dispersion curve for a two-layer system is shown in Figure 3.5. Two distinct branches are obvious. First, up to a wavelength approximately equal to H (thickness of the uppermost layer), the velocity of propagation is independent of wavelength. At wavelengths greater than H, the dispersive characteristic of surface waves (i.e. variation of velocity with wavelength) is strongly evident. Therefore, if one simply generates high-frequency (short-wavelength) waves and assumes that the properties of the uppermost layer are uniform, the modulus of the top layer, G, can be very easily determined from

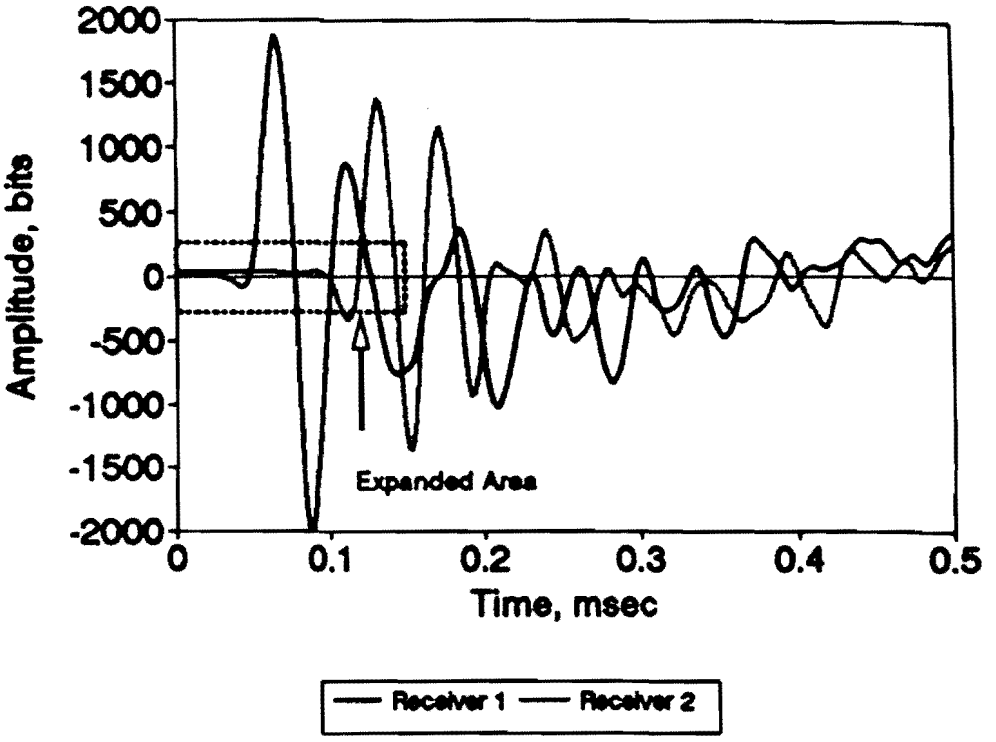

a) Measured

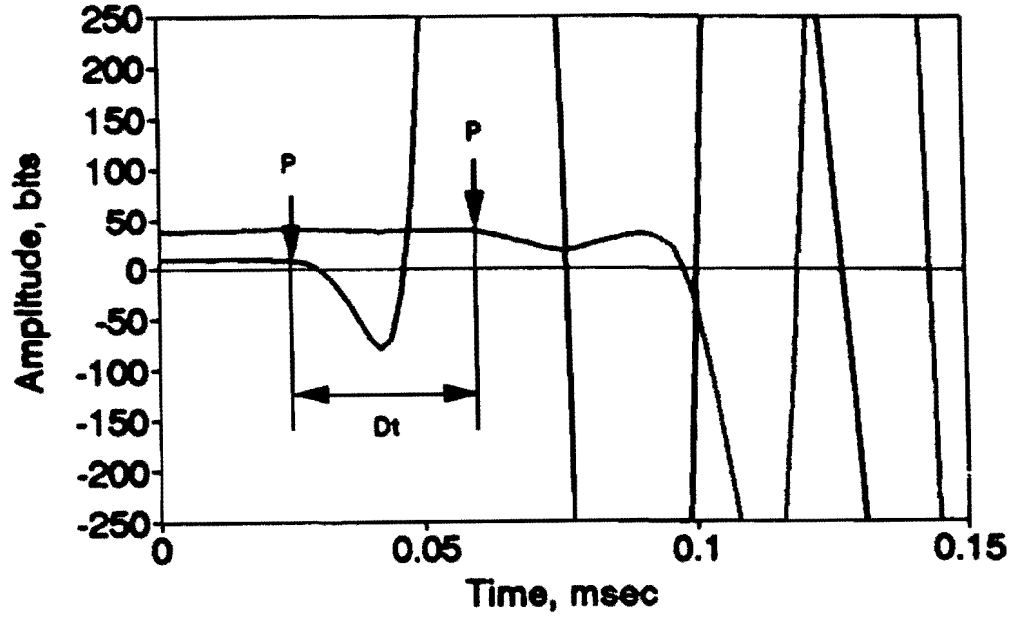

b) Expanded

Figure 3.4 - Typical Time-Domain Records Used in Ultrasonic Body Wave Method

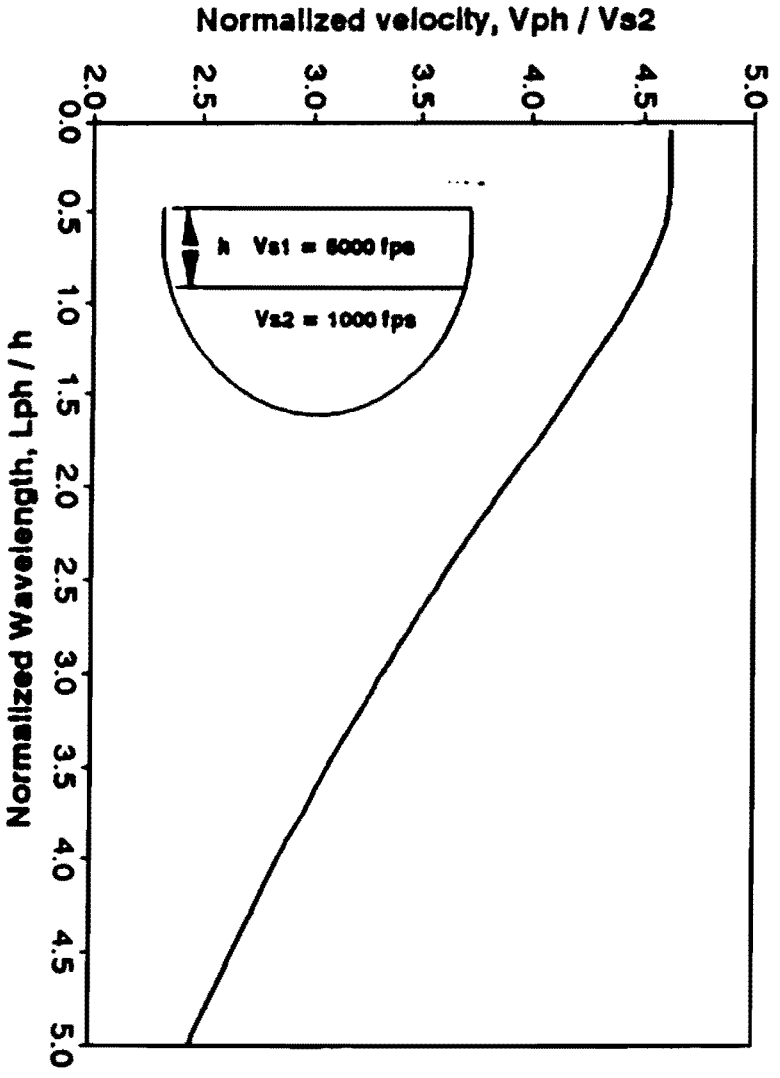

Figure 3.5 - An Idealized Theoretical Dispersion Curve for a Rigid Pavement

$$E = \rho\,[K\,V_{ph}]^2, \tag{3.6}$$

where

$$K = 1.13 - 0.16\nu. \tag{3.7}$$

In the above equations, V_{ph}, ρ, and ν are the velocity of surface waves, mass density, and Poisson's ratio, respectively. An estimate of the thickness of the surface layer can be made by determining the wavelength above which the surface wave velocity is constant.

The methodology can be simplified even further. Assuming that the stiffness of the top paving layer is constant, Equation 3.4 can be written as

$$\phi = [360D / V_{ph}]\,f = m\,f. \tag{3.8}$$

Equation 3.8 represents a linear relationship between the phase of the cross power spectrum and frequency, provided the phase velocity is constant. Thus, one can easily determine V_{ph} by performing a least-squares linear regression over the high-frequency region of the cross power spectrum and obtaining the slope of the best-fit line.

This method uses the time signals measured with the two accelerometers (see Figure 3.2). These two signals are Fourier-transformed, and their ratio is calculated in the form of the transfer function. Since the transfer function is a complex-valued function, each point can be represented by its magnitude and phase. With this method, only the phase of the transfer function is utilized.

A phase spectrum for the time records shown in Figure 3.2 is shown in Figure 3.6a. The phase oscillates between $-\pi$ and $+\pi$ radians (-180 and +180 degrees). This is the standard method of presenting phase data because the detail variation in the data can be observed in a small space.

The data shown in Figure 3.6a show a clear trend of variation in phase with frequency up to a frequency of about 30 kHz. The coherence function associated with this record is shown in Figure 3.6b. The coherence is almost equal to one up to a frequency of 35 kHz. Above a frequency of 35 kHz, the data are of low quality and not usable.

To obtain the shear modulus of the top layer, a complex-valued curve-fitting process—using the coherence as the weighing function—was utilized (see Nazarian and Desai, 1993). The result of the operation is shown in Figure 3.7. The actual and fitted curves compare quite favorably up to a frequency of 30 kHz.

In the next step, the phase is "unwrapped;" that is, an appropriate number of cycles is added to each phase. The unwrapped phase for the "wrapped" phase shown in Figure 3.7 is shown in Figure 3.8. The slope of the line is more or less constant with frequency.

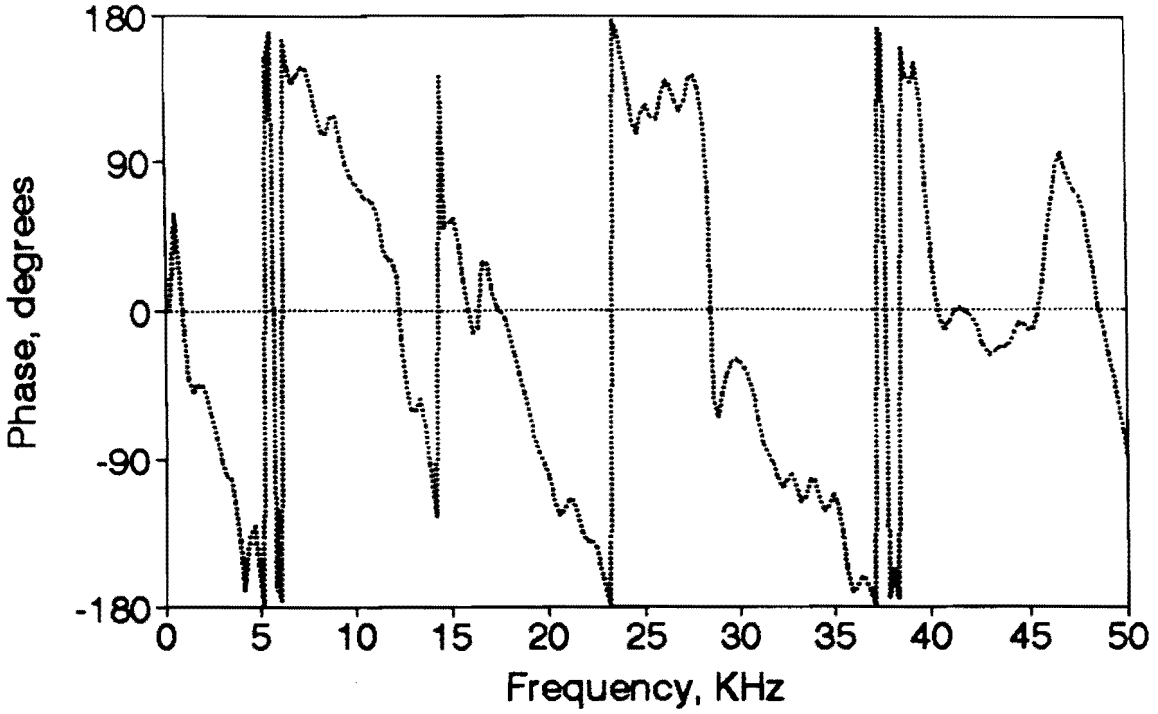

a) Transfer Function

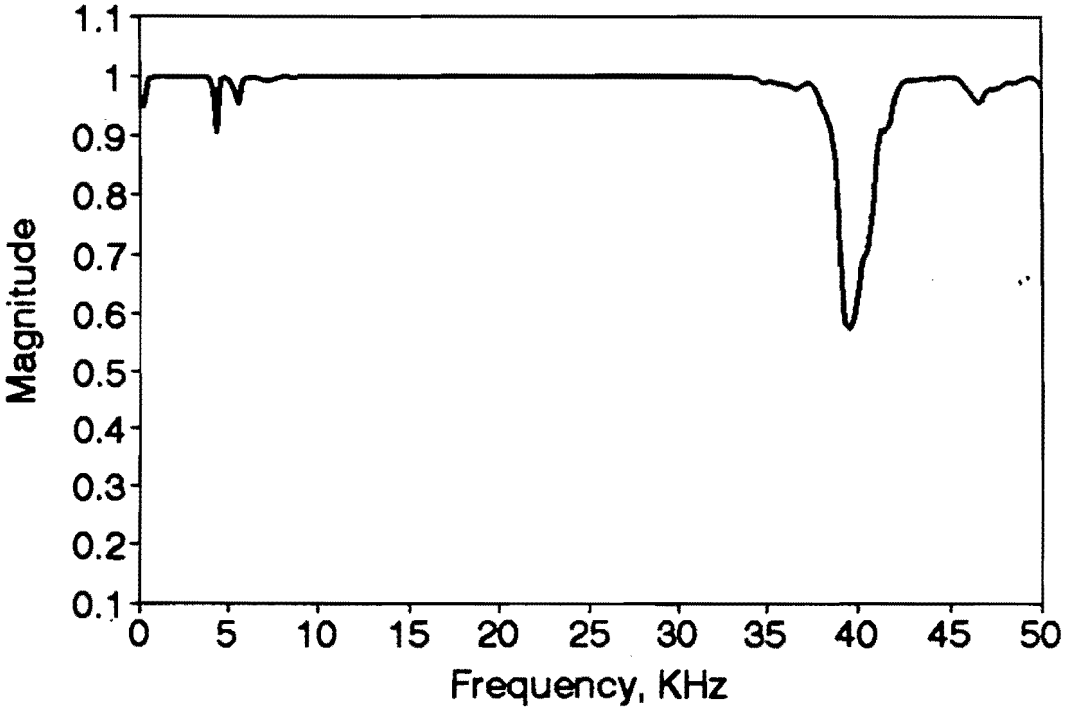

b) Coherence Function

Figure 3.6 - Typical Spectral Functions Used in Ultrasonic Surface Wave Method

Finally, a line is fitted to the curve in the range of frequencies corresponding to wavelengths shorter than the thickness of the top layer. The slope of the line can be utilized to determine the shear modulus (see Equation 3.8).

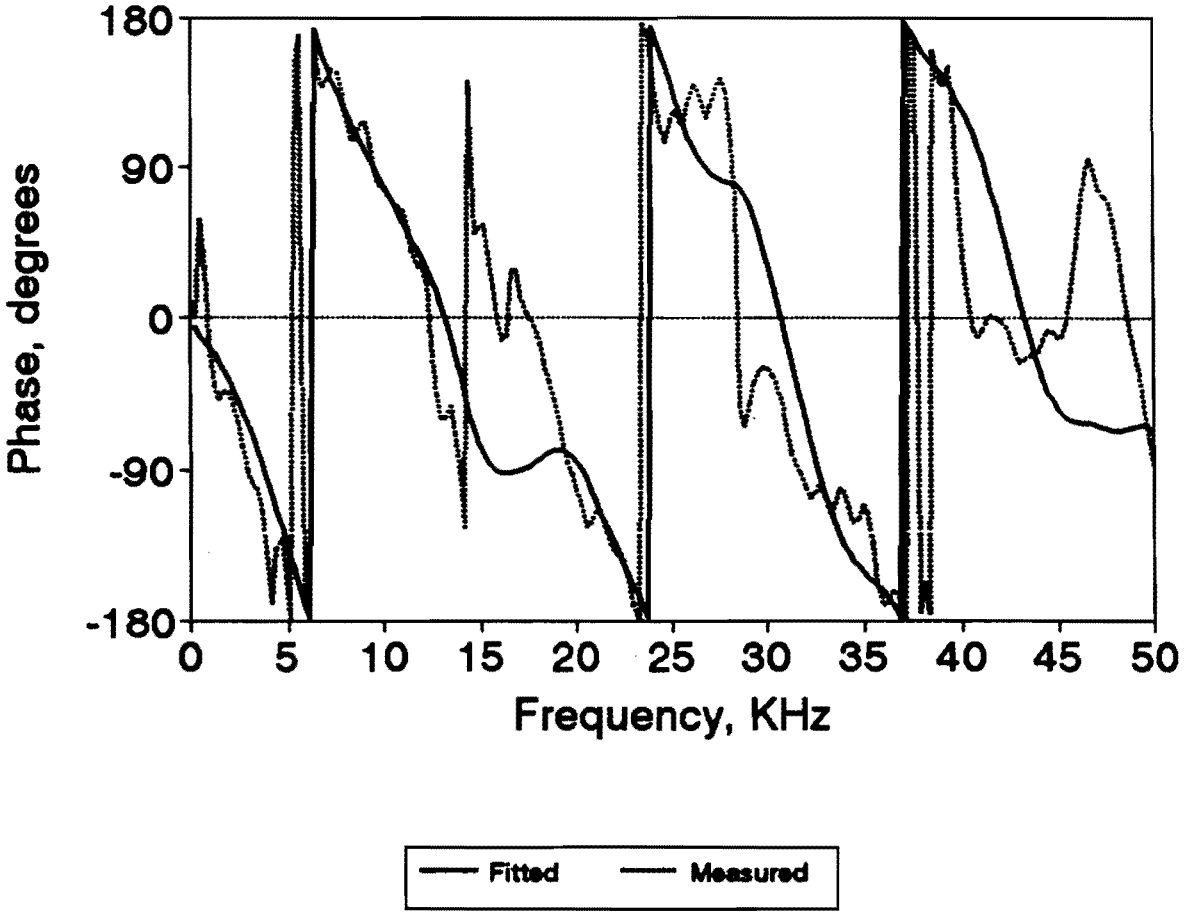

Figure 3.7 - Comparison of the Measured and Fitted Transfer Functions

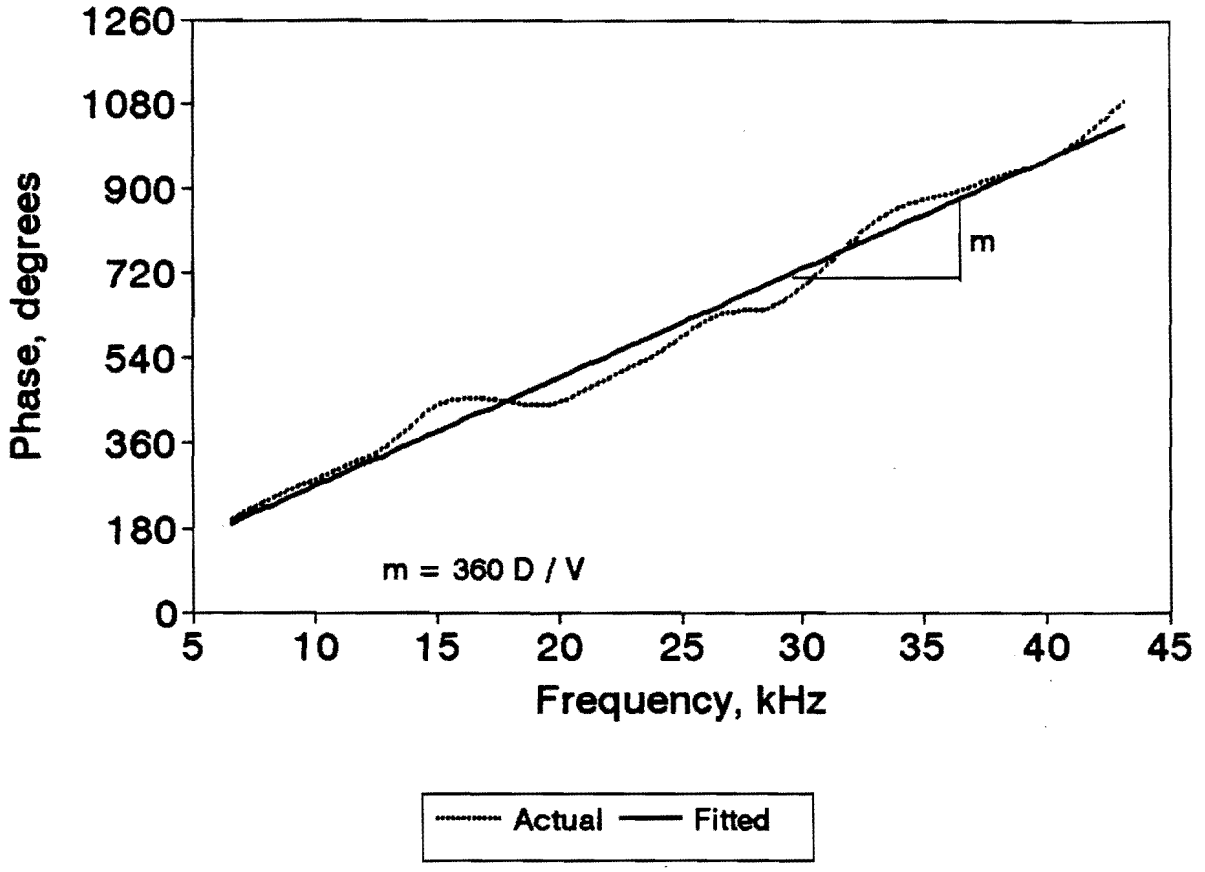

Figure 3.8 - Unwrapped Phase Obtained from Transfer Function Shown in Figure 3.6

4

Conceptual Design

This chapter deals with the general considerations for the design of the Lunch Box. The discussion is broken into two topics. The first deals with how the Lunch Box will be used and how an operator is expected to interact with it. The second topic deals with directions that can be taken when the current prototype is adequately tested.

Operation of the Lunch Box

The measurements made by the Lunch Box, as well as the software used in data collection, are a subset of those used in the Seismic Pavement Analyzer (SPA). The two near transducers are repackaged into a hand-portable system, and the source is reduced in size and energy to make reliable wave propagation measurements at 15 cm, rather than 200 cm. The user interface software, as well as the data acquisition software and database format, is similar to that used in the SPA but has less options and requires fewer measurements.

The Lunch Box is operable from a computer located in a vehicle. This computer is tethered to the hand-carried transducer unit through a cable that carries power to the accelerometers and hammer and returns the measured signal to the data acquisition board in the computer. This configuration was necessary because of the high power requirements and size of the analog-to-digital acquisition board.

Based on our experience with the prototype SPA, we will continue to provide three levels of interaction with the user. These three are (1) the technician performing routine data collection, (2) the experienced engineer or supervisor configuring the Lunch Box for collection, and (3) an engineer or technician performing interactive collection or running diagnostics.

Data collected with the Lunch Box will be formatted for entry into a relational database. In addition to the paving layer modulus and thickness, the data will include position, time, an equipment identifier, and diagnostic messages. Data formatted for or retrieved from the database may be loaded into a spreadsheet for flexible visual displays, analytical calculations, or report generation.

Future Lunch Box Design Considerations

Several aspects of the current Lunch Box design will need to be improved, and several extensions are likely to be considered useful. Subsequent sections discuss hardware modifications and a reduction in software capability needed to make the device truly portable, as well as changes necessary to extend measurement capabilities.

Portability

The physical configuration of the Lunch Box is most strongly limited by the currently available PC-based data acquisition boards. The 1 MHz sampling requirement results in a high consumption of power and on-board acquisition memory. To date, we have found only full-size plug-in PC cards, drawing 12 watts of power, that can handle the A/D needs. The resulting physical package with the needed power supplies would be very cumbersome to run, even with the use of vehicle battery power.

When we find a low-power A/D system, we can package the A/D board, with a single-board 486SLC computer and serial-port LCD readout, in a battery-operated package. Another option would be to have a power tether to the vehicle.

Extension of Capability

The similarity between the SPA and Lunch Box permits software advances developed for the SPA to be readily incorporated into the Lunch Box. Software improvements developed and tested on the TxDOT SPA should improve the quality of compressional wave and ultrasonic surface wave velocity estimates. The addition of a third accelerometer would also improve velocity estimates and permit multi-layer interpretations on multi-course pavements.

Transducers and Source

The major mechanical components of the Lunch Box version of the Seismic Pavement Analyzer (SPA) are schematically depicted in Figure 4.1 (also see Figure 3.1). These include the near and far accelerometer (A and B), the electric solenoid used as a source (C), the amplifier board (D), the solenoid firing board (E), and the computer system (F).

The major electrical components of the Lunch Box are schematically shown in Figure 4.2. These include power supplies, a computer for data acquisition and analysis, signal conditioning electronics, and control electronics. The following subsections describe the individual elements of each of these three systems in greater detail.

Transducer Mounting

The main structural member holding the transducers and source is a thick steel plate mounted to the base of the box holding the electronics. Rubber vibration isolators decouple the accelerometers (A and B, Fig. 4.1) from the steel plate above 100 Hz. The source is directly mounted to the steel plate. A heavy plate was deliberately chosen to act as a reaction mass to couple the source energy into the concrete and force the accelerometers onto the pavement surface.

An electrical solenoid is used as a source of vibration energy. A small spring return rod in the center of the solenoid hits the concrete when an electrical current is applied through the solenoid for several milliseconds. The contact time of the rod with the concrete is primarily a function of the mass of the rod: in this case, the contact time is in the range of 100 microseconds.

Electronic Components

A general schematic of the total electronic system, including the interface with the computer, is shown in Figure 4.2. Transducer signals collected in the box are on the upper right. The first level of boxes to the left of the transducer signals are electronics located in the transducer box and include the source control and accelerometer amplifiers. The accelerometer signals are routed to the analog-to-digital (A/D) converter in the computer. The parallel printer port on the back of the computer is used to control the solenoid source. The complete electronic package is run on linear supplies on an inverter connected to the 12-volt system of the tow vehicle.

Computer Specifications

The data acquisition software of the Lunch Box requires either an i386 or i486 IBM-PC AT or equivalent computer with a floating-point processor, 4 megabytes of RAM, two expansion slots, one serial port, and one parallel port. If the data acquisition software is run on the same machine which holds the data acquisition board, a Hercules color graphics adaptor (CGA), enhanced graphics adaptor (EGA) or video graphics adaptor (VGA), graphics monitor, and keyboard are required.

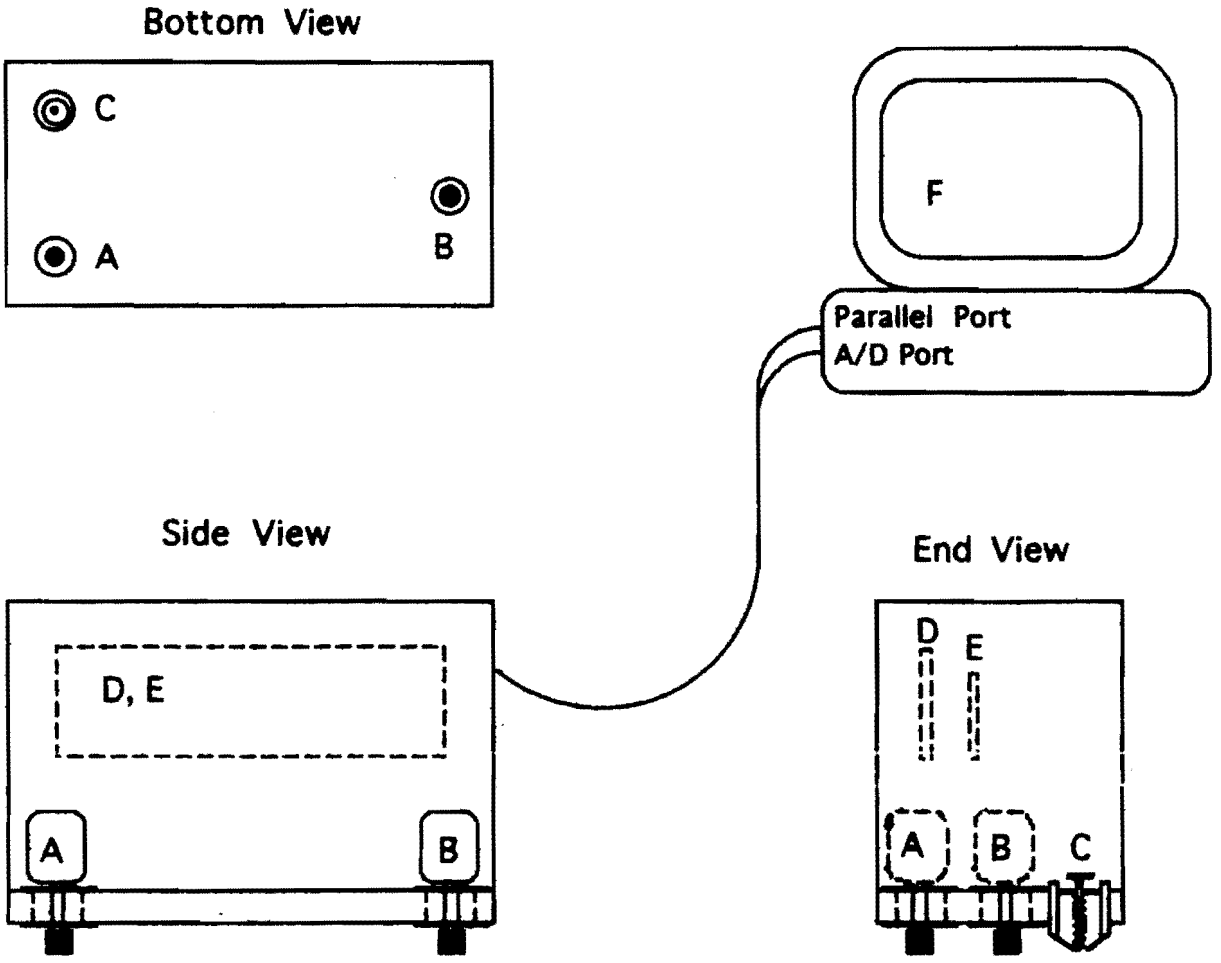

Figure 4.1 - Major Mechanical Components of the Lunch Box

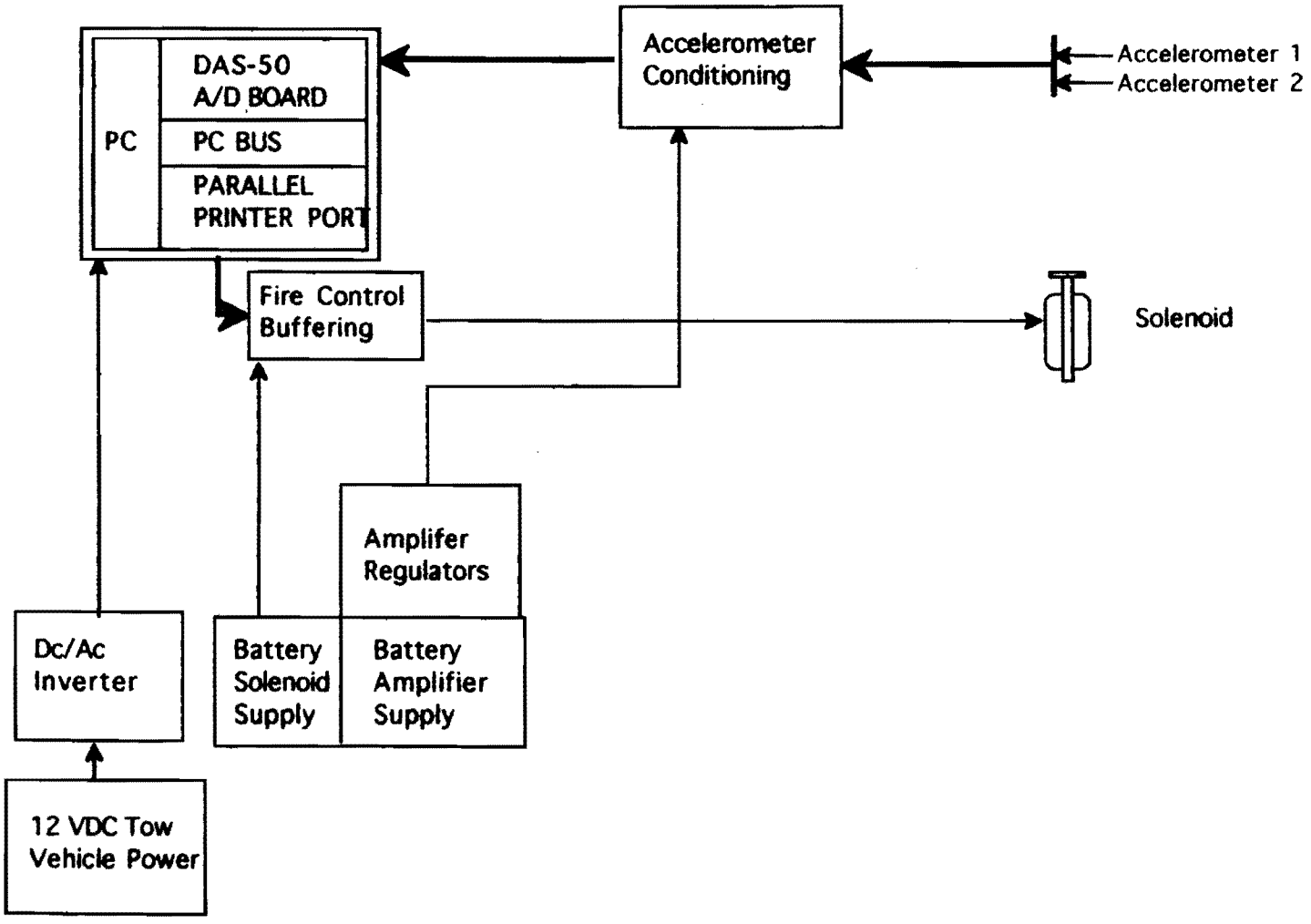

Figure 4.2 Electronic system layout.

The user interface software of the Lunch Box runs on an IBM-PC XT- or AT-equivalent computer having Hercules, CGA, or EGA/VGA graphics, 640 Kb RAM, two 720 Kb floppy disk drives, and three serial ports. An AT with a hard disk and floating-point chip would be highly desirable but not necessary to increase the speed of operation in analysis-intensive operations.

5

Case Studies

In the remainder of this report, the results from several case studies are presented to demonstrate the versatility and shortcomings of the device. It should be mentioned that several experiments were carried out to evaluate the repeatability of the results. This was done by repeating the test on one point numerous times. In virtually all cases, the reported results were identical.

Case I - UTEP Concrete Slab

A series of tests was carried out on a slab located on the UTEP campus. The slab measures 12 m in length, 2.4 m in width, and approximately 140 mm in thickness. Its schematic is shown in Figure 5.1. The results of tests carried out at 30-cm intervals along a longitudinal line are discussed.

Typical time records recorded by the first accelerometer about 75 mm from the source are shown in Figure 5.2a for test points 9 through 15 (2.7 m to 4.5 m from the edge). The results (except for test point 14) are quite repeatable.

Similar time records for the second receiver are shown in Figure 5.2b. With the exception of those for test point 14, the results are repeatable.

The time records were used to determine the compression wave velocity, V_p, of the concrete. The variation in V_p with test point is shown in Figure 5.3 and Table 5.1. The average value is about 4,000 m/sec, with a variation of about 10 percent.

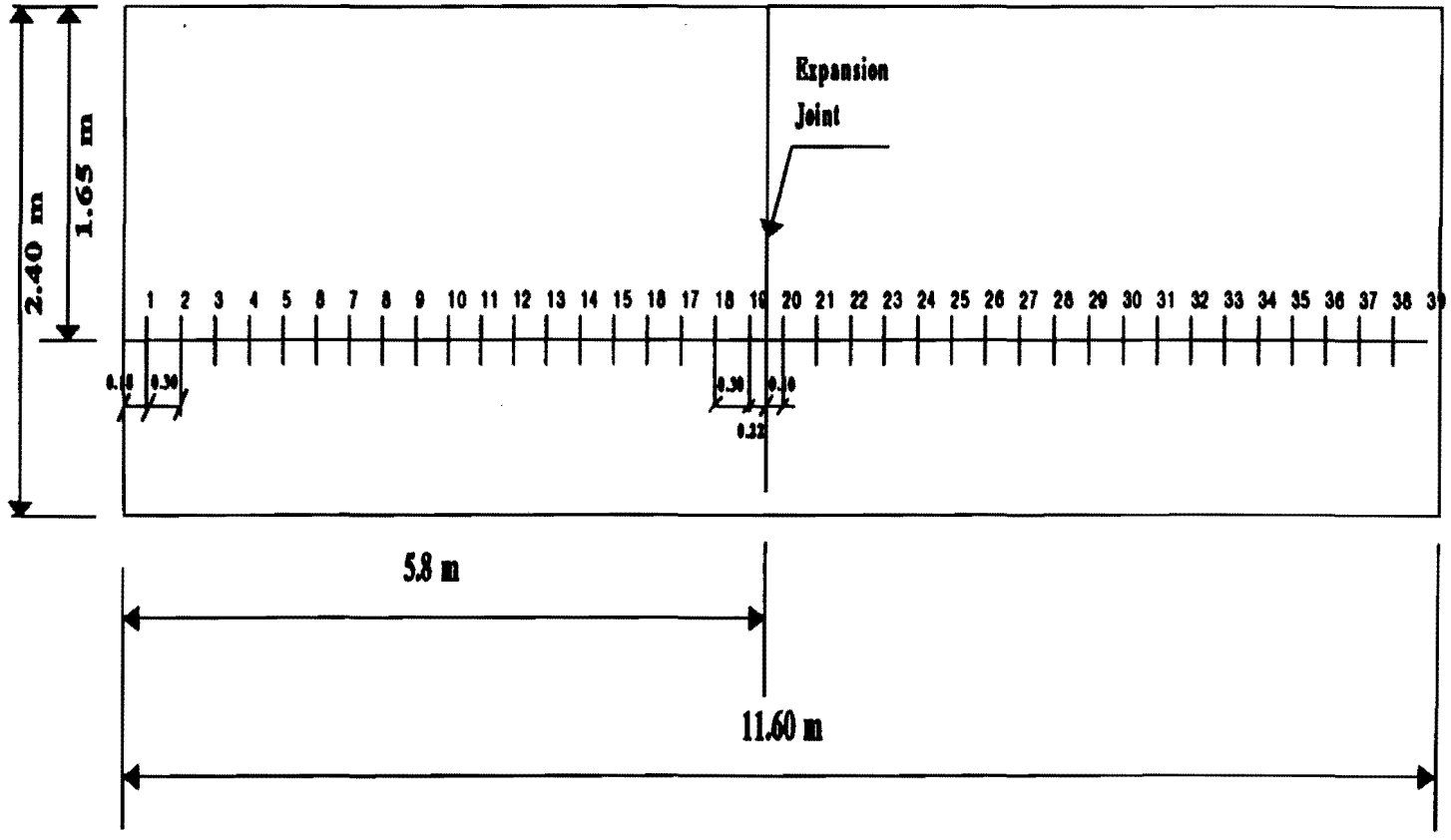

Figure 5.1 - Plan View of UTEP Slab

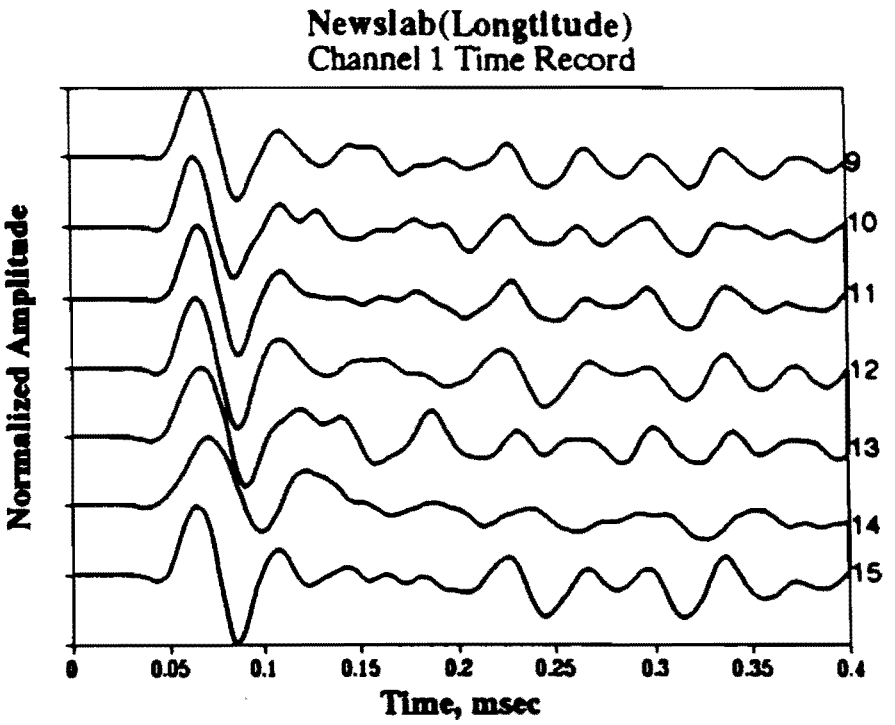

a) Receiver 1

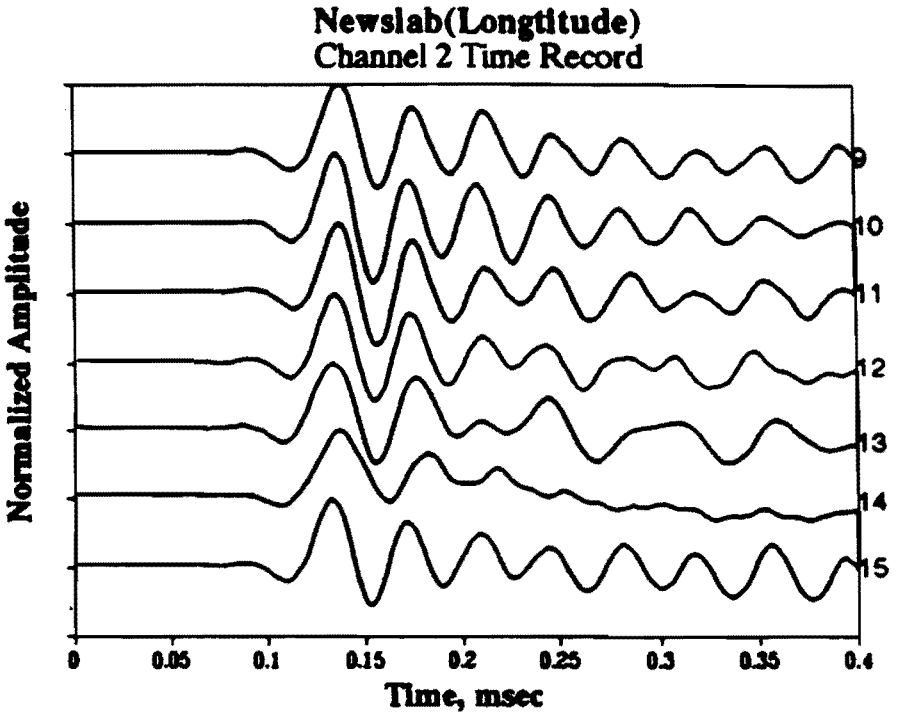

b) Receiver 2

Figure 5.2 - Typical Time Records Measured on UTEP Slab

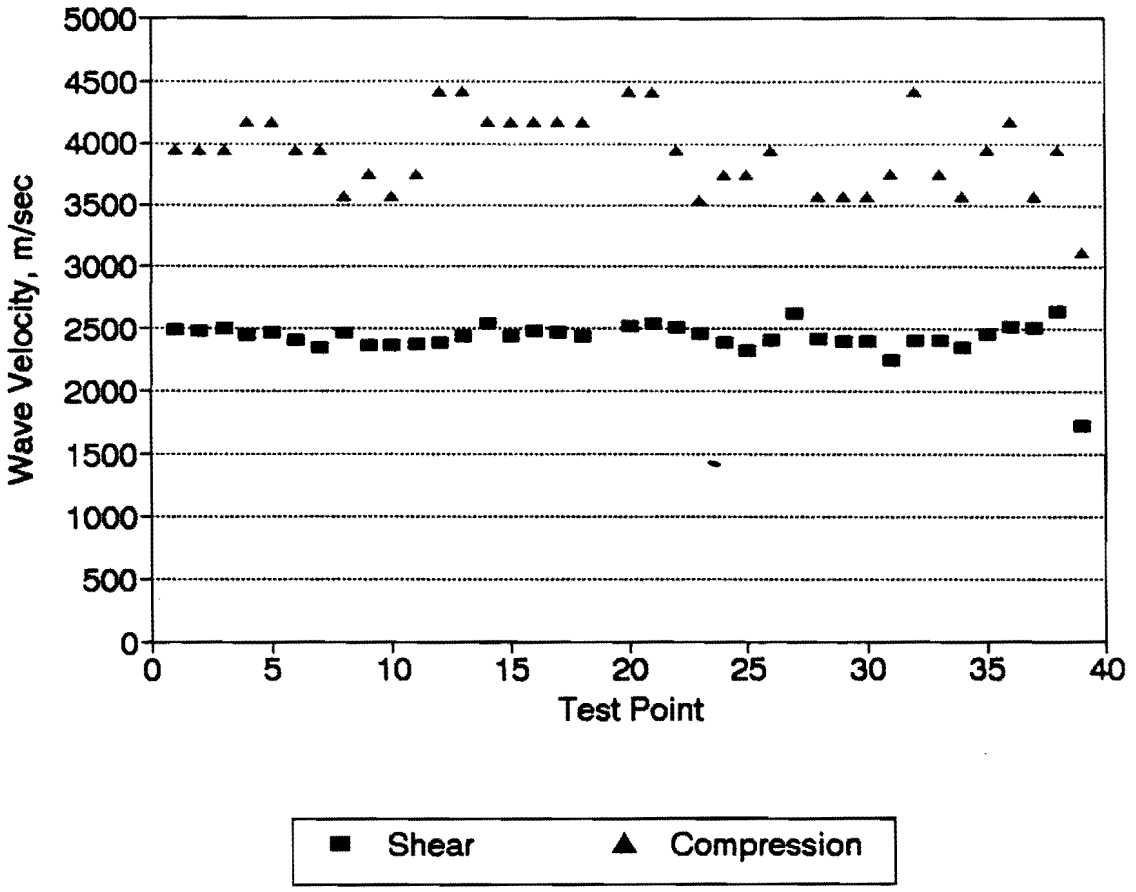

Figure 5.3 - Variation in Wave Velocities along UTEP Slab

Table 5.1 - Summary of Results Obtained along UTEP Slab

Test Point	Wave Velocity, m/sec		Modulus, GPa		Thickness, mm
	Shear	Compression	Shear	Young's	
1	2488	3947	15	39	135
2	2476	3947	15	39	137
3	2490	3947	16	39	122
4	2446	4167	15	43	145
5	2462	4167	15	43	152
6	2400	3947	14	39	137
7	2339	3947	14	39	137
8	2467	3571	15	32	128
9	2362	3750	14	35	135
10	2363	3571	14	32	131
11	2376	3750	14	35	137
12	2386	4412	14	49	159
13	2433	4412	15	49	153
14	2536	4167	16	43	145
15	2439	4167	15	43	150
16	2479	4167	15	43	152
17	2468	4167	15	43	142
18	2434	4167	15	43	145
19	--	--	--	--	147
20	2519	4412	16	49	146
21	2535	4412	16	49	151
22	2504	3947	16	39	142
23	2454	3541	15	31	129
24	2384	3750	14	35	137
25	2324	3750	14	35	130
26	2402	3947	14	39	139
27	2623	--	17	--	139
28	2416	3571	15	32	118
29	2391	3570	14	32	120
30	2396	3570	14	32	118
31	2251	3750	13	35	126
32	2400	4412	14	49	151
33	2405	3750	14	35	128
34	2357	3571	14	32	126
35	2450	3947	15	39	142
36	2512	4167	16	43	140
37	2500	3571	16	32	128
38	2645	3947	17	39	137
39	1731	3125	7	24	108

Also shown in Figure 5.3 is the variation in the shear wave velocity obtained from the ultrasonic-surface-wave (USW) method with test point. The shear wave velocities were obtained from phase spectra similar to those shown in Figure 5.4. The shear wave velocities exhibit much less variation, indicating that this method may be more robust than the ultrasonic-body-wave (UBW) method used to determine compression wave velocities. However, the measured shear and compression wave velocities follow the same general pattern.

The amplitude spectra from the impact-echo method are included in Figure 5.5 for test points 9 through 15. Once again, the records are similar.

The thicknesses at each point, determined using the return (resonant) frequency and the compression wave velocity measured with the ultrasonic-body wave method, are shown in Figure 5.6. The nominal thickness of the slab, as well as the anticipated bounds associated with the accuracy of the method, are also shown in the figure. Most thicknesses fall within the prescribed bounds.

Also shown in the figure are the thicknesses estimated by converting the shear wave velocities measured with the USW method to compression wave velocities, assuming a Poisson's ratio of 0.18 (see Chapter 2 for the relationship). The estimated thicknesses are concentrated much closer to the nominal thickness and exhibit much less variation. This is expected, since the results from the USW method exhibited less variability than those of the UBW method.

Finally, the shear and compression wave velocities were converted to shear and Young's moduli, respectively. These values, which are presented in Table 5.1, can easily be utilized to determine the quality of the concrete.

Case II - Doniphan Drive

A series of tests was carried out at ten points along a newly re-constructed section of Doniphan Drive in El Paso, TX. The ten test points were 1 m apart. The cross-section of the road consisted of 200 mm of PCC, over an asphalt-treated base and a clayey subgrade.

The typical time-domain records for the two receivers are shown in Figure 5.7. The first arrivals are similar for practically all of the records. Some high frequency oscillation is detected for some records, including test point 5. Similarly, the phase spectra from the USW tests are shown in Figure 5.8 to demonstrate the level of repeatability of results obtained for different points. The results are once again repeatable.

The shear and compression wave velocities are demonstrated in Figure 5.9 and are included in Table 5.2. The compression wave velocities of different points are more or less similar. No values for points 3 and 4 are reported because no appreciable compression wave energy could be detected for the records.

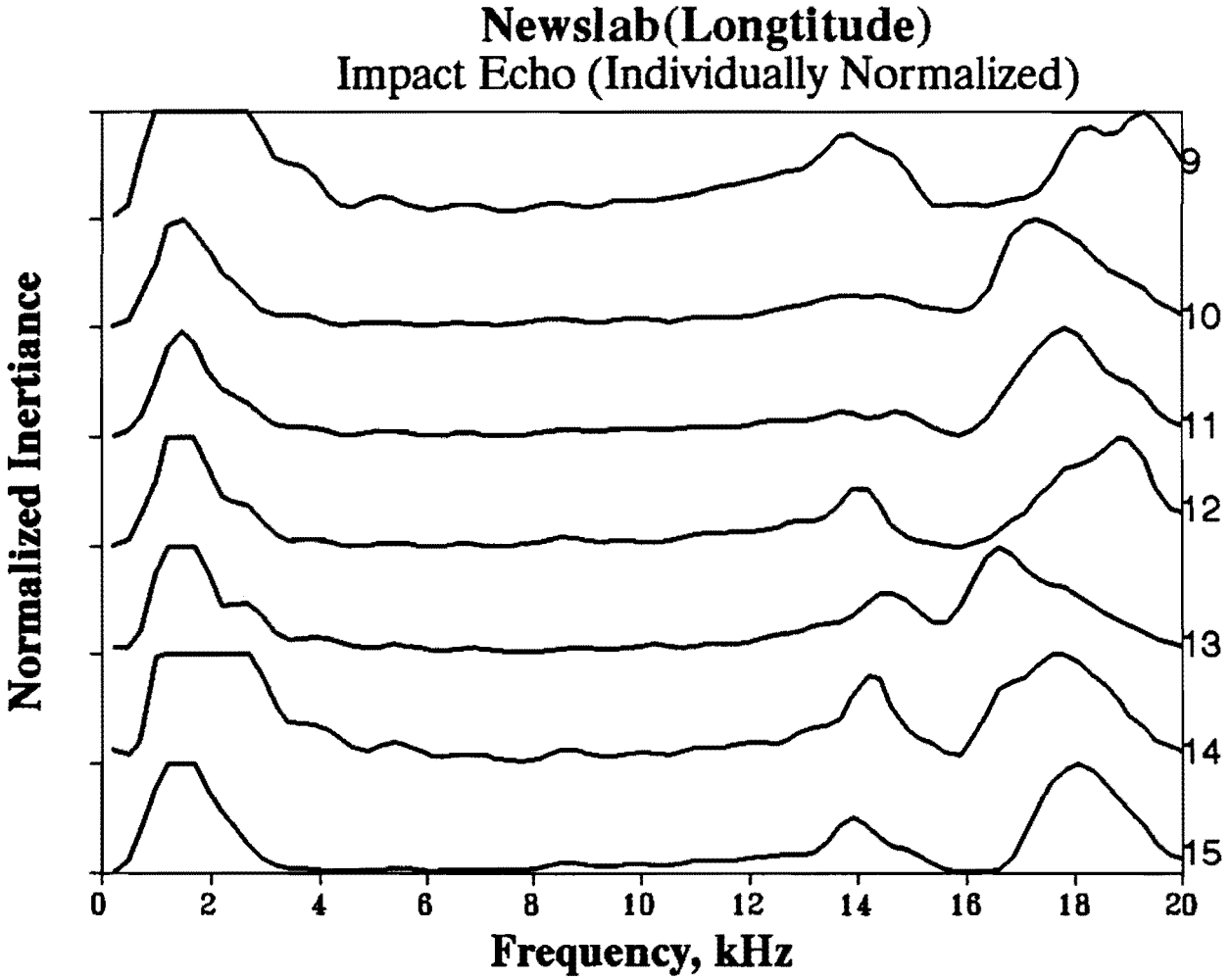

Figure 5.4 - Typical Phase Spectra Measured with USW Method on UTEP Slab

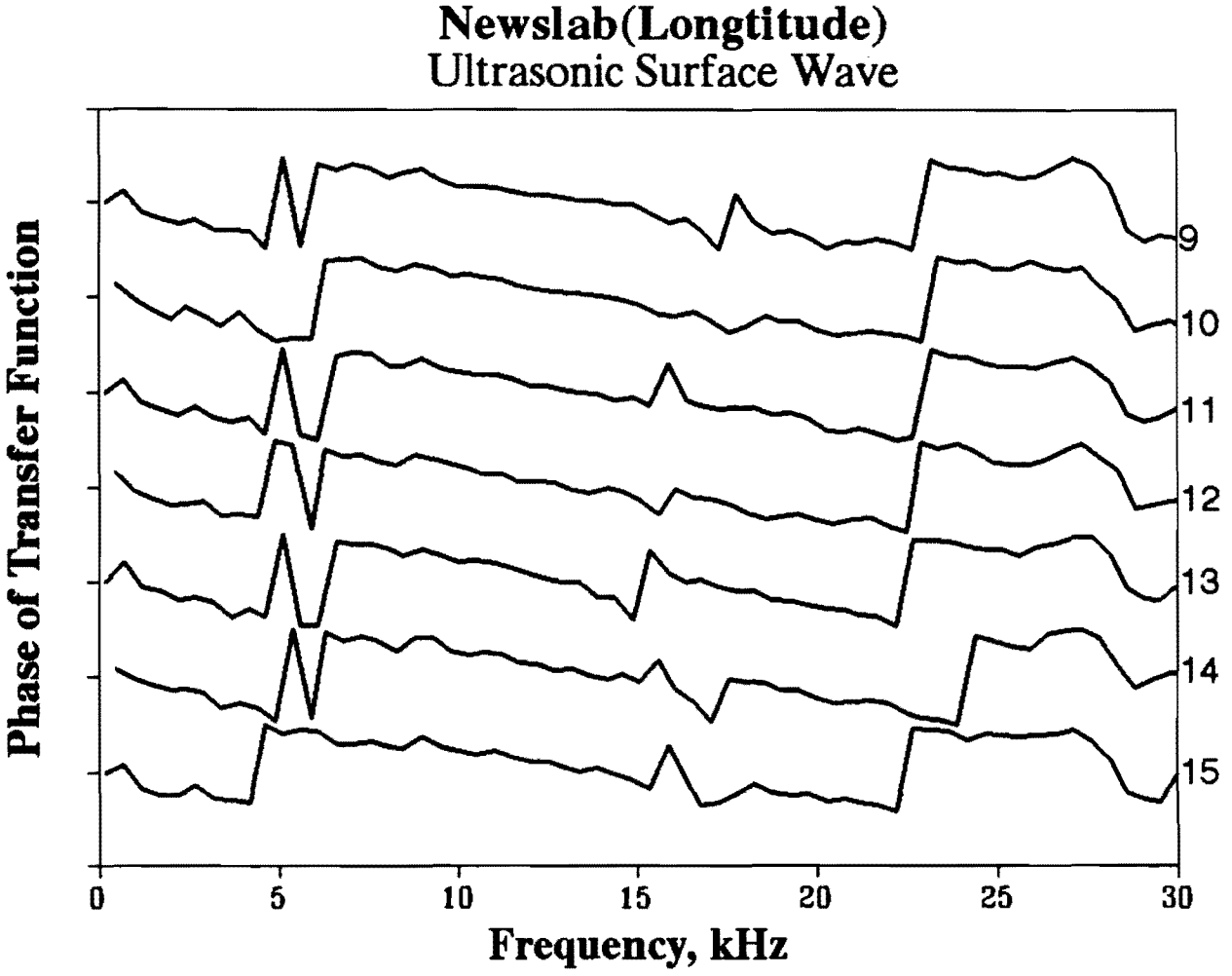

Figure 5.5 - Typical Amplitude Spectra Measured with IE Method on UTEP Slab

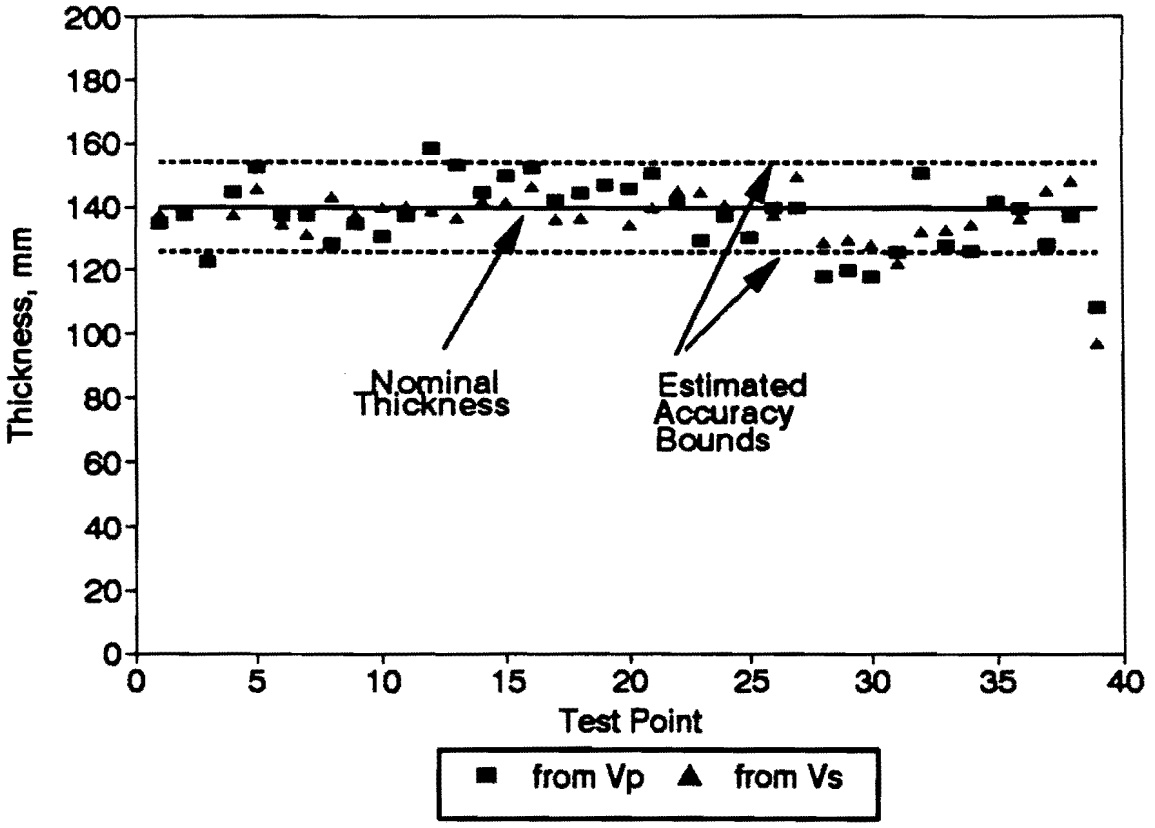

Figure 5.6 - Variation in Thickness Measured along UTEP Slab

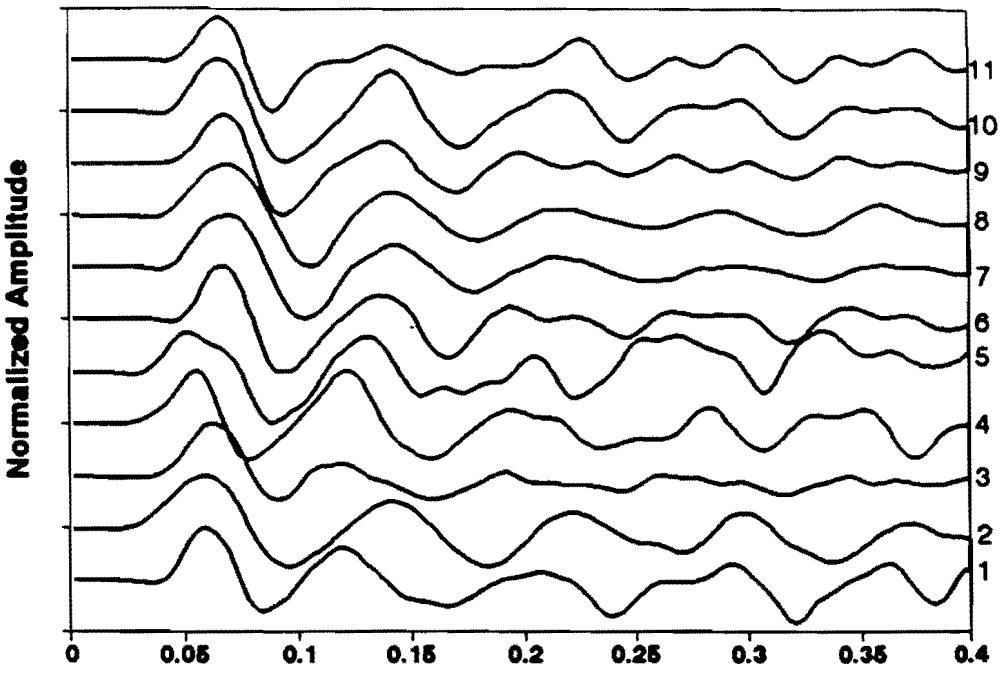

a) Receiver 1

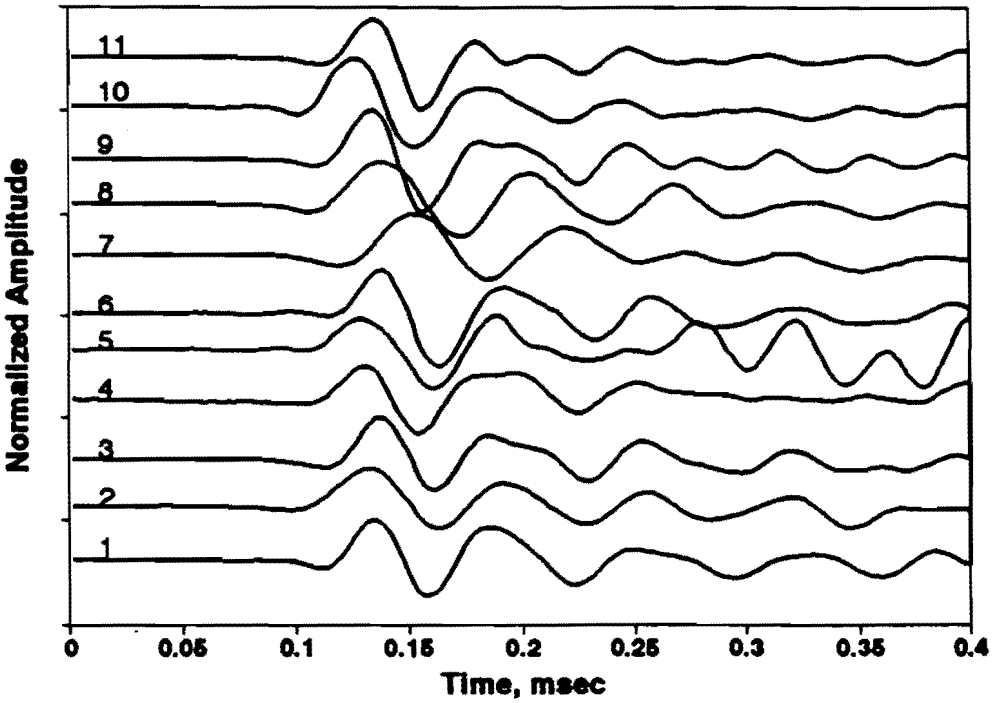

b) Receiver 2

Figure 5.7 - Time Records Measured on Doniphan Drive

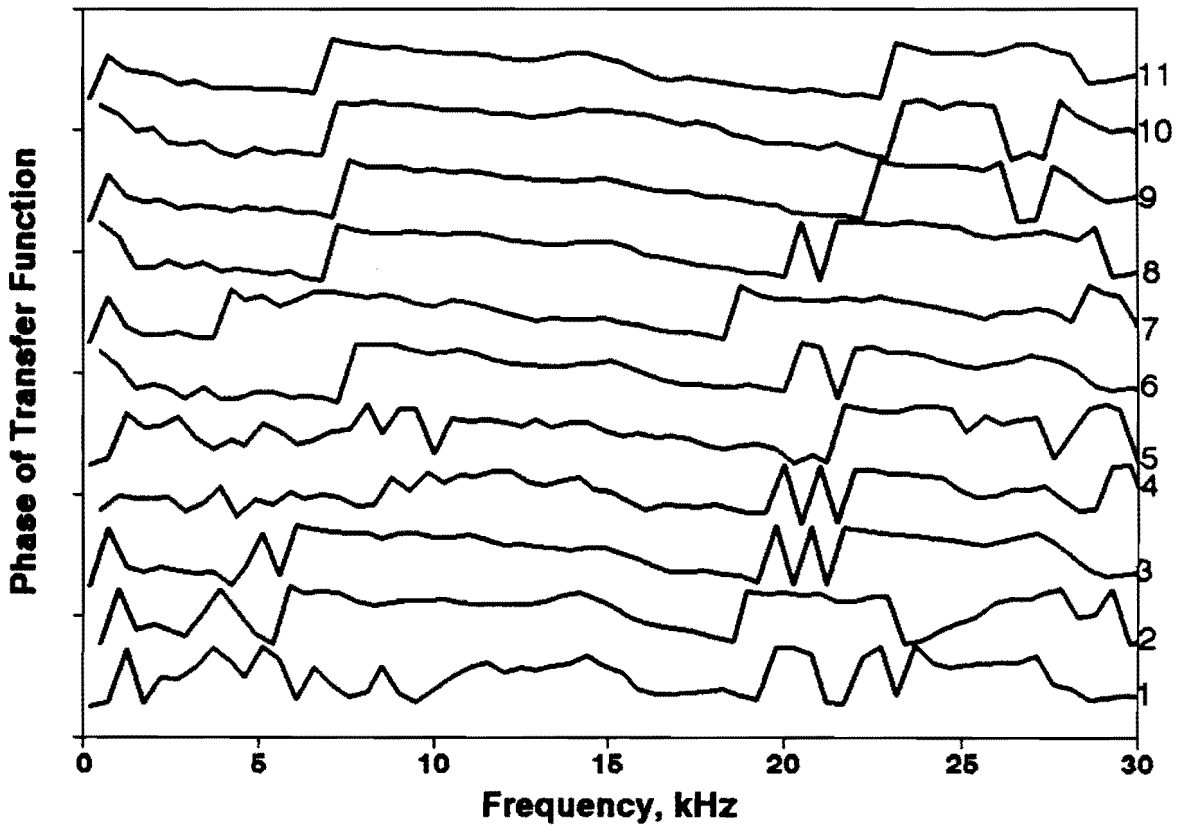

Figure 5.8 - Phase Spectra Measured with USW Method on Doniphan Drive

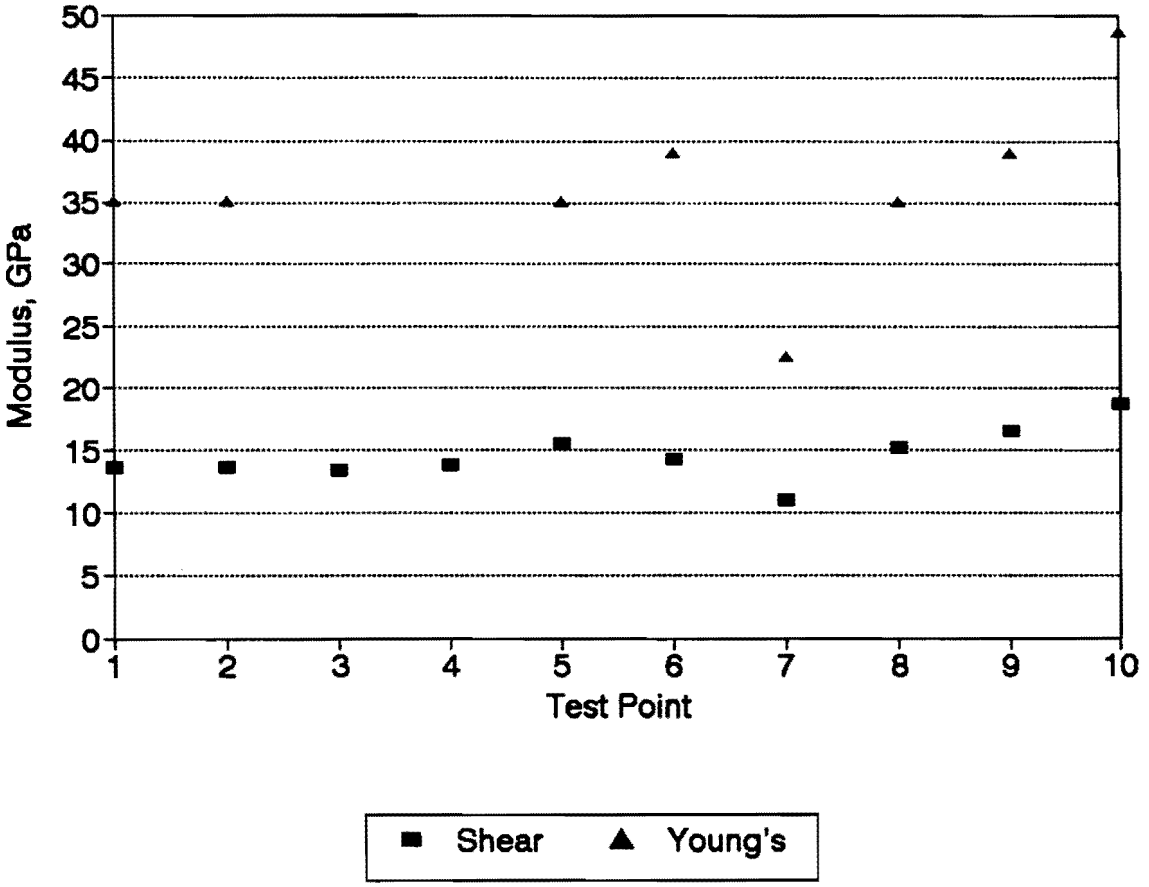

Figure 5.9 - Variation in Wave Velocities Measured along Doniphan Drive

Table 5.2 - Summary of Results Obtained along Doniphan Drive

Test Point	Wave Velocity, m/sec		Modulus, GPa		Thickness, mm
	Shear	Compression	Shear	Young's	
1	2341	3750	14	35	208
2	2334	3750	14	35	192
3	2322	–	13	–	208
4	2355	–	14	–	–
5	2492	3750	16	35	197
6	2394	3947	14	39	180
7	2096	3000	11	23	166
8	2467	3750	15	35	171
9	2566	3947	16	49	–
10	2739	4412	19	49	201

The shear wave velocities once again exhibit less variation than the compression wave velocities, indicating that the USW method may be more robust. Shear wave velocities are available for all data points.

The amplitude spectra from impact-echo tests performed on different test points are shown in Figure 5.10. One representative record is depicted in Figure 5.11. A large peak is apparent at a frequency of about 14 kHz. The reason for this peak is not very apparent. Two hypotheses being pursued are (1) electronic noise in the system and (2) resonance due to pavement-receiver interaction. An extensive effort is under way to understand and minimize this phenomenon.

The actual peak corresponding to the thickness of the layer is also marked in the figure. Even though the amplitude is small, it is detectable for most records. Due to the large magnitude associated with the noise, the resonant frequency could not be determined for points 9 or 4.

The thicknesses estimated from the compression wave velocities and shear wave velocities are demonstrated in Figure 5.12. Most values are within the target range of thicknesses. Once again, the thicknesses obtained from the shear wave velocities and an assumed Poisson's ratio of 0.18 seem closer to the nominal thickness of the layer.

Case III - Asphalt Section

To determine if the Lunch Box is operable on AC pavements, a small experiment was carried out at a site in Dallas, Texas. The motivation behind this exercise was to determine if the device could be used as a quality-control tool on this type of material. The results for one data point are shown here as an example.

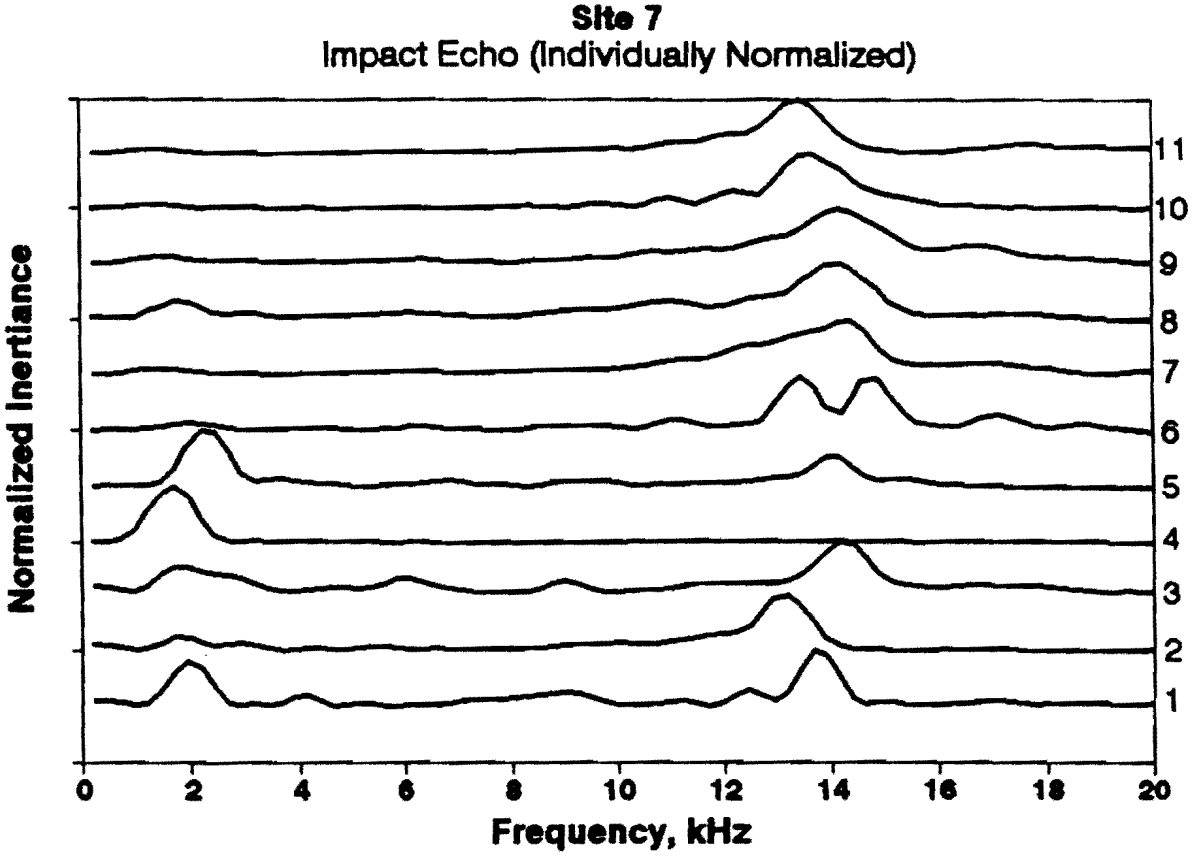

Figure 5.10 - Amplitude Spectra Measured with IE Method on Doniphan Drive

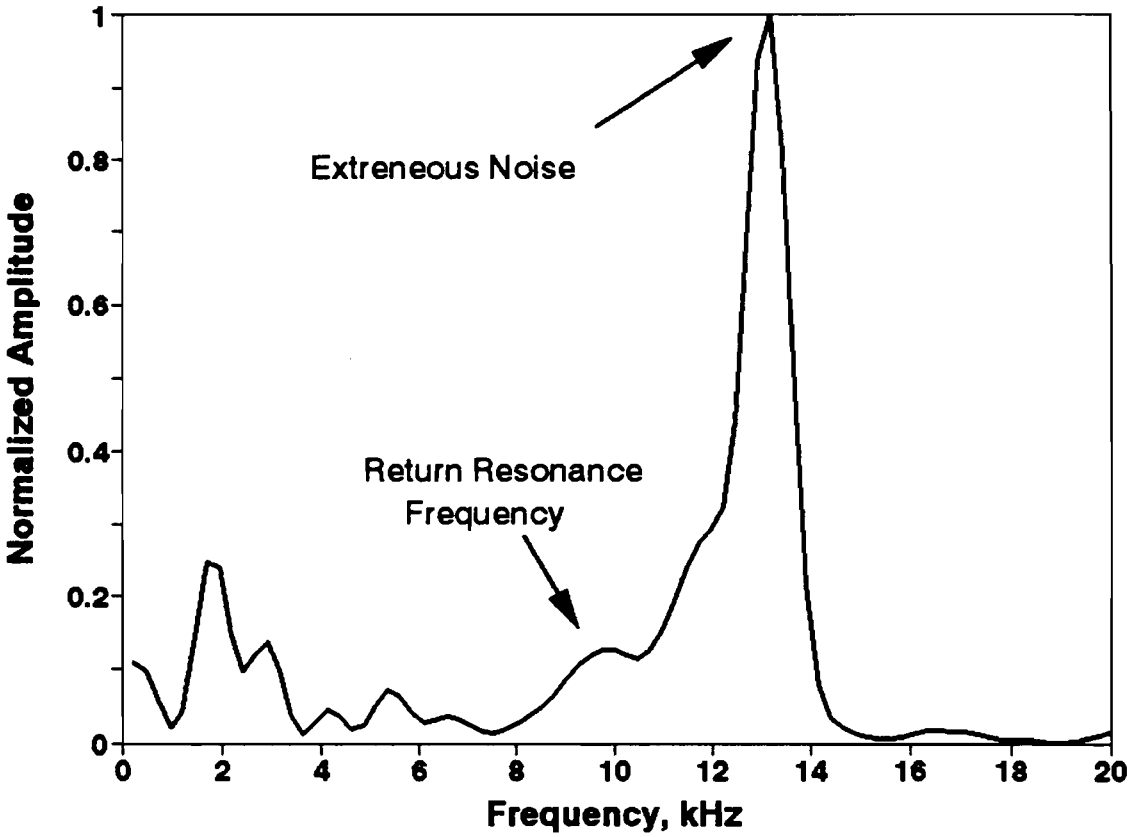

Figure 5.11 - Representative Amplitude Spectra Measured on Doniphan Drive

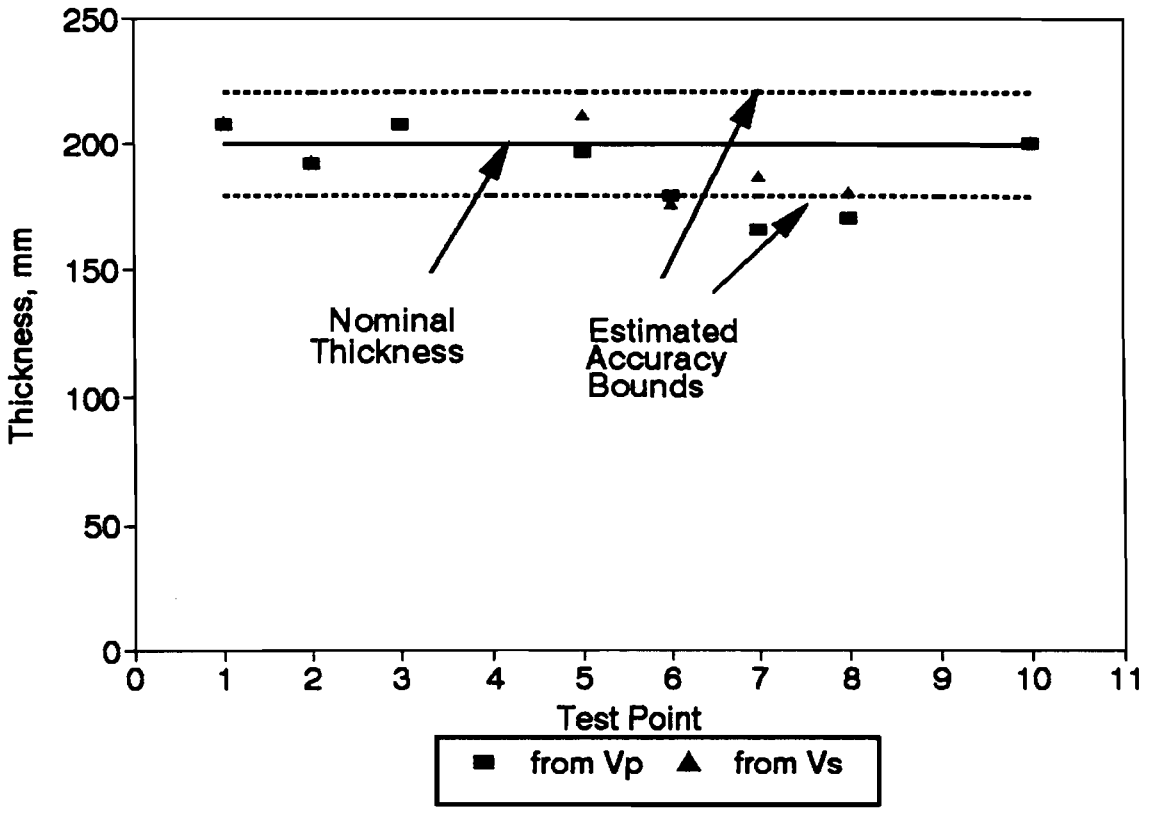

Figure 5.12 - Variation in Thickness of Slab Measured along Doniphan Drive

Due to the nature of the project, tests had to be carried out very close to the edge of the asphalt, where the pavement was relatively steep. The Lunch Box could not be properly seated under such a condition. In locations where the device could be securely placed, it worked satisfactorily. However, more tests need to be conducted to determine the conditions under which the device can be effectively used on flexible pavements.

Typical time-domain records for one point are shown in Figure 5.13. The arrivals of the compression wave velocities are quite clear and are marked as "P" on the record. For a spacing of 150 mm between receivers, a compression wave velocity of 2780 m/sec was obtained. This is quite reasonable for an AC layer.

The phase spectrum and the coherence function, simultaneously measured at the same point, are shown in Figure 5.14. The quality of the data, as judged from the coherence function or trend of the phase spectrum, is excellent. The shear wave velocity associated with this data is about 1450 m/sec, again representative of such material.

From the shear and compression wave velocities, the Poisson's ratio is about 0.30, which seems reasonable for the material tested.

As expected, the thickness of the AC layer cannot be determined with the device. This is because of limitations of the minimum measurable thickness and the small impedance mismatch between the AC and base materials.

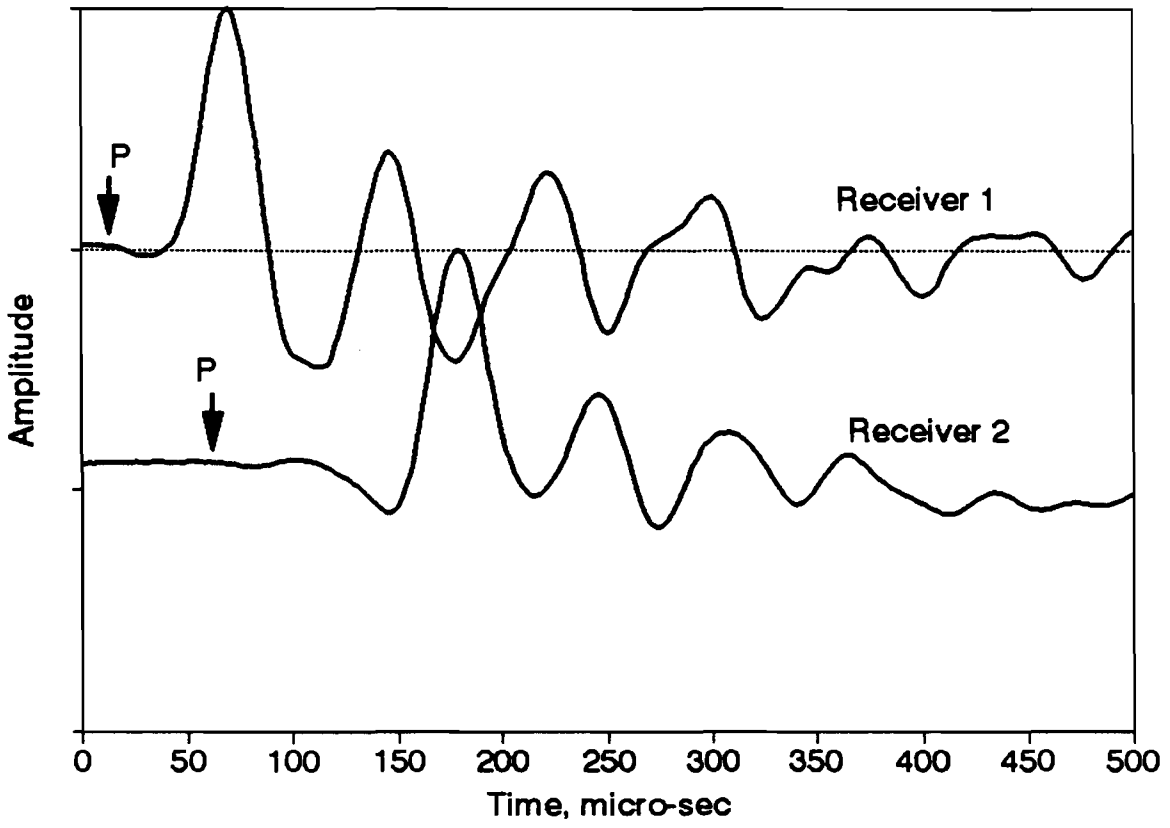

Figure 5.13 - Typical Time-Domain Records Measured on an AC Pavement

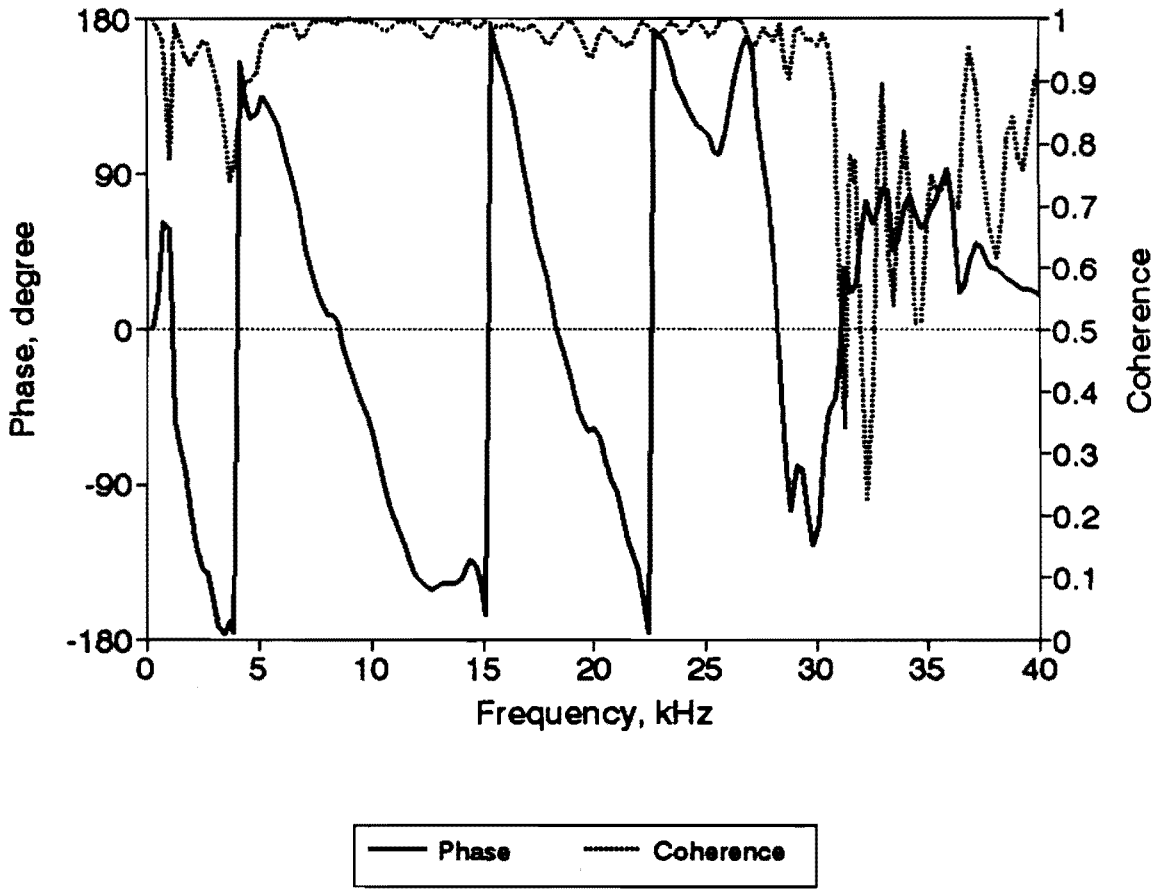

Figure 5.14 - Typical Spectral Functions Measured with USW method on an AC Pavement

6

Closure

This report highlights the efforts to develop a new nondestructive device used to evaluate Portland cement concrete.

The goal of the project was to develop a portable device that could determine the shear and compression wave velocities of concrete, as well as its thickness. These goals were achieved with a device called the Lunch Box.

Summary

The principles of measurement, along with the Lunch Box's approach, were clearly defined. The theoretical background of each testing technique was discussed. This document also presented an overview of the conceptual design of the Lunch Box, as well as a description for the implementation of the design. Typical data collection and reduction procedures were discussed using comprehensive examples.

Several case studies determined the accuracy, applicability, and limitations of the Lunch Box. A slab recently constructed at the University of Texas at El Paso was tested. The results obtained from a field site in El Paso, Texas were also reported. A feasibility study was also carried out to determine the applicability of the device to AC pavements.

Conclusions

At the end of this project, it can be concluded that

1. The Lunch Box is useful for evaluating PCC slabs.

2. The Lunch Box can, in most cases, easily, accurately, and repeatably collect and reduce data.

3. The Lunch Box is field worthy, rugged, and can handle different climatic conditions.

4. The final versions of the software and hardware function relatively well.

Recommendation for Future Developments

A fully functional prototype Lunch Box has been developed and tested. As with any prototype, further testing and development are required to establish confidence in the operation, durability, and usefulness of the device. The following aspects of the Lunch Box would benefit from additional testing:

1. The long-term reliability of the electrical and mechanical components of this application is unknown because the latest prototype has been in use for only six months. So far the device has performed with minimum problems; however, continued and extensive testing is required to establish the level of reliability. The hardware and software should be tested under a wide variety of pavement conditions to induce software and hardware failures, with consequent improvement in the robustness of these components.

2. The Lunch Box has been tested on a limited set of pavement conditions. The robustness of moduli and thickness estimation algorithms should be investigated.

References

1. Bolt, B.A. 1976. Nuclear Explosions and Earthquakes, W.H. Freeman and Co., San Francisco, 309 pp.

2. Miller, G.F. and H. Pursey. 1955. "On the Partition of Energy between Elastic Waves in a Semi-Infinite Solid." In *Proceedings*, International Conference on Microzonation for Safer Construction: Research and Application (Society of Exploration Geophysicists, Seattle, WA) Vol. 2, 545-58.

3. Nazarian, S. and M. Desai. 1993. "Automated Surface Wave Testing: Field Testing," *Journal of Geotechnical Engineering* (American Society of Civil Engineers, New York) 119, no. GT7:1094-112.

4. Richart, F.E., Jr., Hall, J.R., Jr., and R.D. Woods. 1970. Vibrations of Soils and Foundations, Prentice-Hall, Inc., Englewood Cliffs, NJ, 414 pp.

5. Sansalone, M. and N.J. Carino. 1986. "Impact-Echo: A Method for Flaw Deflection in Concrete using Transient Stress Waves." Report NBSIR 86-3452. National Bureau of Standards, Gaithersburg, MD.

6. Willis, M.E. and M.N. Toksoz. 1983. "Automatic P- and S-Velocity Determination from Full Wave Form Digital Acoustic Logs." *Geophysics* 48, no. 12: 1631-44.